CHARACTERIZATION OF RPGR VARIANTS AND THEIR ROLE IN INHERITED RETINAL DEGENERATION

A Dissertation

by

RACHEL NICOLE WRIGHT

Submitted to the Office of Graduate Studies of
Texas A&M University
in partial fulfillment of the requirements for the degree of

DOCTOR OF PHILOSOPHY

August 2011

Major Subject: Genetics

Characterization of RPGR Variants and Their Role in Inherited Retinal Degeneration

CHARACTERIZATION OF RPGR VARIANTS AND THEIR ROLE IN INHERITED RETINAL DEGENERATION

A Dissertation

by

RACHEL NICOLE WRIGHT

Submitted to the Office of Graduate Studies of
Texas A&M University
in partial fulfillment of the requirements for the degree of

DOCTOR OF PHILOSOPHY

Approved by:

Chair of Committee,	Michael F. Criscitiello
Committee Members,	Gladys Ko
	Brian Perkins
	C. Jane Welsh
Intercollegiate Faculty Chair,	Craig Coates

August 2011

Major Subject: Genetics

ABSTRACT

Characterization of RPGR Variants and Their Role in Inherited Retinal Degeneration.

(August 2011)

Rachel Nicole Wright, B.S., Texas A&M University

Chair of Advisory Committee: Dr. Michael F. Criscitiello

Retinitis Pigmentosa (RP) refers to a group of inherited retinal dystrophies resulting from progressive photoreceptor degeneration and accumulation of intra-retinal pigment-like deposits. X-linked forms of RP are frequently caused by mutations in the *retinitis pigmentosa GTPase regulator* (*RPGR*) gene. The RPGR transcript undergoes complex alternative splicing to express both constitutive ($RPGR^{ex1-19}$) and $RPGR^{ORF15}$ variants. Although RPGR is thought to play a role in ciliary function, little is known about the physiological significance of expressing two distinct groups of variants. This study compares $Rpgr^{ex1-19}$ and $Rpgr^{ORF15}$ expression in developing photoreceptors using immunoblot analysis and immunohistochemistry, assesses ciliary affinity in adult photoreceptors by protein fractionation, examines Rpgr function in transgenic mouse models and identifies a novel $Rpgr^{ORF15}$ binding partner using a yeast two-hybrid screen.

Our data reveal that Rpgr expression undergoes dynamic temporal regulation during retinal development and indicates variability in ciliary localization of Rpgr variants in adult photoreceptors. Utilization of distinct Rpgr variants during stages of photoreceptor

development suggests independent roles. Further examination of Rpgr function using transgenic mouse models over-expressing either the $Rpgr^{ex1-19}$ or $Rpgr^{ORF15}$ variant reveals that despite normal ciliary localization, an excess of $RPGR^{ex1-19}$ results in atypical accumulation of Rpgr in photoreceptor outer segments, abnormal photoreceptor morphology and severe retinal degeneration. The data indicate that the constitutive variant cannot substitute for Rpgr function in photoreceptors and suggest that proper maintenance of the Rpgr isoform ratio is critical to photoreceptor viability.

Using mouse retinal cDNA in a yeast two-hybrid screen with the C-terminus of the $Rpgr^{ORF15}$ variant, we identified a novel variant of whirlin as an interacting partner. Mutations in whirlin result in Usher syndrome, a disorder characterized by hearing loss and RP. RT-PCR and immunoblot analysis were used to confirm the presence of selected candidate partners in the retina and interaction was confirmed by pull-down assays and co-immunoprecipitation from retinal homogenate. Immunohistochemistry showed co-localization of RPGR and whirlin within photoreceptors and identified isoform specific localization of whirlin. These findings indicate that whirlin binds $Rpgr^{ORF15}$ and that this novel isoform may be required for photoreceptor function, thus providing a potential mechanism for the RP phenotype observed in Usher syndrome.

DEDICATION

This work is dedicated to my mentor, Dr. Dong-Hyun Hong, who sadly passed away on December 24, 2009, prior to completion of this dissertation. I am honored to have the opportunity to carry on his research.

ACKNOWLEDGEMENTS

I would like to thank my mentor, Dr. Don Hong, for his dedication to my education and for his high expectations. He has not only trained me at the bench but has also taught me many valuable life lessons.

I would also like to thank my committee chair, Dr. Michael Criscitiello, for allowing me the opportunity to finish my doctoral research project. This dissertation would not have been possible without his encouragement and support.

My committee members, Dr. Gladys Ko, Dr. Brian Perkins, and Dr. Jane Welsh, also deserve recognition for their guidance and support and for going above and beyond to help me succeed. I am especially grateful to Dr. Perkins for his efforts in preparation and publication of my manuscripts.

Thanks also go to my friends and colleagues and the department faculty and staff for making my time at Texas A&M University a great experience. I also want to extend my gratitude to the Department of Veterinary Pathobiology for its financial support, and to Dr. Fuller Bazer, our interim department head, for generously allowing me the opportunity to complete my thesis project.

Finally, thanks to my parents for the opportunities that they have afforded me, to my husband for his love and encouragement, and to my baby girl for her patience while I completed my dissertation and prepared for my defense.

NOMENCLATURE

CC	Connecting cilia
DFNB31	Deafness, autosomal recessive 31
IS	Inner segment
LCA	Leber's congenital amaurosis
MBP	Maltose binding protein
OS	Outer segment
RCC1	Regulator of chromatin condensation
RP	Retinitis pigmentosa
RPGR	Retinitis pigmentosa GTPase regulator
RPGRIP	Retinitis pigmentosa GTPase regulator-interacting protein
RPE	Retinal pigment epithelium
USH2D	Usher syndrome, type 2D
WHRN	Whirlin

TABLE OF CONTENTS

CHAPTER Page

LIST OF FIGURES

FIGURE Page

CHAPTER I

INTRODUCTION AND LITERATURE REVIEW

"*The eyes are the window of the soul."* – English Proverb

Vision is arguably our most fundamental sensory system. Associations have historically been made between blindness and enlightenment, and the loss of vision has long been viewed as a tragedy. Used as a metaphor in classic Greek tragedies and old English proverbs, the gift of sight has long been described based upon the practical experience of humanity.

Vision and ocular anatomy

When looking into someone's eyes, we easily see several features. The most predominate of these are the pupil, which is the aperture that allows light to enter the eye, and the surrounding iris. While the iris is more commonly known as the pigmented feature that gives us our eye color, from a functional standpoint, it is a circular muscle that controls the size of the pupil so that more or less light is allowed to enter the eye.

This dissertation follows the style of *Journal of Biological Chemistry*.

The pupil and iris are both covered by a clear, external lens called the cornea, which is the most powerful lens in the eye and forms a continuous encasing with the external covering of the eye, known as the sclera or "white of the eye" (1) .

What we do not see hidden beneath this exterior are the transparent lens located behind the iris and the chambers of fluid between the cornea and iris, between the iris and lens and between lens and retina. The first two chambers, known as the anterior chamber and posterior chamber, respectively, are filled with aqueous humour, while the third vitreous chamber is filled with a more viscous fluid known as the vitreous humour.
Although all parts of the eye are important for image acquisition, the retina is the most essential, functional part of the anatomy (1). Since Santiago Ramón y Cajal's anatomic description of the cell types that constitute the vertebrate retina (2,3), it has been the goal of many visual scientists to understand the functional organization of this specialized neural tissue. Modern technological advances, including the advent of electron microscopy, microelectrode recording techniques, and immunohistochemistry, have recently allowed for rapid advancement in our understanding of the neural circuits employed by each functional component.

Introduction to retinal biology

The retina, which is part of the central nervous system, forms from out pouching from two sides of the neural tube during embryonic development. Known as the primordial optic vesicles, these out pouches fold back on themselves to form the optic cup with the

inner most layer of the cup, the diencephalic neuroectoderm, developing into the retina and the outside epithelial layer remaining a single layer of cells later called the retinal pigment epithelium. Development of the sensory neurons in the retina begins as early as the optic vesicle stage with highly coordinated inductive and migratory events. Cell division and subsequent migration of cell nuclei toward the inner surface give rise to the various cell types and multi-layered organization of the retina, with development proceeding in an inside to outside manner. Essentially, the retina develops into a piece of brain tissue that detects a diverse assortment of stimuli from the outside world. Its highly organized structure, with discrete layers of cells and complex intercellular connections, is required for transduction of external stimuli to the cerebral subcortex and cortex, which process retinal input to fashion the full range of visual perception that we experience (4-6).

When light rays enter the eye, they are focused through the transparent cornea and lens on the retina. In the human eye, the central focal point of the visual axis is called the fovea, which is located slightly more nasally than the optic axis (longest sagittal distance between the front of the cornea and the furthest posterior part of the eye) and optic nerve head. Although the fovea is unique to the primate retina and some avian species, similar specializations of the central retina known as the *area centralis* and visual streak have evolved in other vertebrate species (4,7).

Cells in the retina are arranged in highly organized, discrete layers, with the bodies of nerve cells arranged in three rows separated by two layers of densely packed synaptic connections. The photoreceptors, which make up the first layer, lie at the back of the retina, against a dark row of melanin containing cells called the retinal pigment epithelium (RPE). The RPE absorbs stray photons of light, preventing their reflection back into the photoreceptors, which would cause blurring of images. The RPE also protects the retina from over exposure to light radiation. The second layer, called the *inner nuclear layer*, is composed of the horizontal, bipolar and amacrine cell bodies. The ganglion cells, which lie near the surface of the retina, make up the third layer. The spaces separating these three layers are also anatomically distinct. The region containing synapses linking the photoreceptors with the bipolar and horizontal cells is known as the *outer plexiform layer*, and the area where the bipolar and amacrine cells connect to the ganglion cells is called the *inner plexiform layer* (4-6).

Photoreceptors are the light sensing neurons in the retina. All vertebrate retinas contain at least two types of photoreceptors: rods and cones, which are both anatomically and physiologically distinct. Cones, which are robust, conical shaped structures, mediate daylight vision and are critical for visual acuity and color discrimination while rods are named for their slender, rod-shaped structure and are generally responsible for low light vision (4,8,9).

Photoreceptors achieve efficient transduction of light to neural signals in part by the elaboration of a specialized organelle for phototransduction known as the outer segment (**Fig. 1.1**). The outer segment is filled with stacked, membranous disks, which are continuously renewed. Older portions of the outer segment are shed at the tip and new membranes are added at the base. Failure to renew the outer segment leads to photoreceptor degeneration (4,10,11).

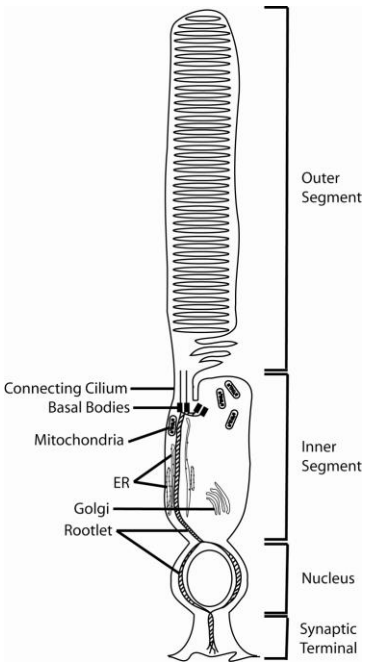

Figure 1.1. Schematic diagram of a rod photoreceptor. Rods are anatomically distinct structures composed of a biosynthetic inner segment and light sensitive outer segment. All protein biosynthesis takes place in the inner segment, and proteins destined for the outer segment are transported via the connecting cilia.

The bilipid membranes of these disks contain light-sensitive, visual pigment molecules, which consist of the chromophore retinal bound to an opsin protein (rhodopsin in rods and conopsin in cones) (12-14). In the dark, retinal is in the form 11-cis-retinaldehyde, the photoreceptors are depolarized, sodium ions flow freely across the cell membranes, and the cells release the neurotransmitter glutamine. Absorption of light photons initiates the isomerization of 11-cis-retinaldehyde to all-trans-retinol, which stimulates transducin to exchange a GDP for a GTP. Transducin with GTP then activates phosphodiesterase, which subsequently changes cGMP into an inactive GMP. Since cGMP acts as a second messenger and opens calcium ion channels, decreasing [cGMP] results in channels closing and the hyperpolarization of the photoreceptor. Thus, when exposed to light, ion channels in the cell membranes close, and the cell goes into a hyperpolarized state and does not release neurotransmitter for as long as the light ensues (9,15).

The light-sensitive outer segments of photoreceptors are connected to the cells' biosynthetic inner segment (cell body) via a junctional structure called the connecting cilium. The inner segment contains all of the cell's organelles (4). Photo pigments (i.e. rhodopsin and cone opsins) and other outer segment proteins are synthesized in the proximal inner segment and are transported via intraflagellar transport (IFT) across the ciliary compartment to the distal outer segment. Passage of proteins through the connecting cilium is critical to the function and maintenance of photoreceptors, thus any impairment of the IFT results in photoreceptor malfunction (16).

Retinitis pigmentosa

Retinitis pigmentosa (RP), the most common cause of inherited blindness, refers to a group of inherited retinal dystrophies that result in progressive retinal degeneration. This clinically and genetically heterogeneous group of disorders affects 1 in every 3,000 to 5,000 individuals (17) and is characterized by photoreceptor cell death and the accumulation of intra-retinal pigment-like deposits, from which the disease gets its name. Symptoms include night blindness, progressive loss of peripheral visual fields, and eventual loss of central vision (18). Recent advances in molecular genetics have provided new insights into the genes responsible for RP. To date, more than 30 different syndromic forms of RP have been reported (19) and more than 60 non-syndromic disease causing loci have been identified (http://www.sph.uth.tmc.edu/Retnet/ provided in the public domain by the University of Texas Houston Health Science Center, Houston, TX), with documented cases of autosomal dominant, autosomal recessive, X-linked, and digenic modes of inheritance (20-24). X-linked forms of RP (XLRP), which have a population prevalence of 1 in 25,000, represent one of the most severe classes of RP cases, as determined by age of onset and disease progression (20,25-27).

X-linked retinitis pigmentosa type 3

Of the six XLRP loci identified, mutations in the *retinitis pigmentosa GTPase regulator* (*RPGR*) gene, which are responsible for X-linked retinitis pigmentosa type 3 (XLRP3) (OMIM312610), account for more than 70% of XLRP and approximately 10% of all RP cases. In addition to accounting for more RP cases than any other RP locus identified to

date, XLRP3 is considered to be the most severe form of RP with symptoms often appearing during the first decade of life (27,28).

Many patients begin to develop difficulties with dark adaptation and night blindness during adolescence. This is often followed by loss of the mid-peripheral visual field and gradual loss of the far peripheral visual field. As the disease progress, they experience tunnel vision, which progresses to complete loss of sight with the loss of central vision (19).

These visual symptoms are indicative of a gradual loss of photoreceptors. In most forms of typical retinitis pigmentosa, loss of rod function proceeds loss of cone function. Thus, night blindness and loss of peripheral visual field are attributed to the degeneration of rods, which mediate dim light vision, and subsequent reduction in cone function is associated with progression of the disease and loss of central vision. There is, however, a tremendous amount of allelic variation and clinical variability associated with *RP3*. Mutations in the *XLRP3* locus have been associated not only with RP as described (25,26,28-30), but also with cone-rod dystrophy (31), cone dystrophy (32) and recessive atrophic macular degeneration (33).

In all RP cases, the outer nuclear layer of the retina, which contains the photoreceptor nuclei, is severely attenuated due to loss of photoreceptors. The inner nuclear layer, which contains the amacrine, bipolar and horizontal cell nuclei, is at first well preserved,

however, many of these cells degenerate as a secondary affect related to the loss of photoreceptor function (19).

Identification of the *XlRP3* locus and its transcriptional heterogeneity

Positional cloning of the human *XLRP3* locus initially identified a gene between *CYBB* and *OTC* in Xp21.1 with 19 constitutive exons spanning 60kb of genomic DNA. The locus encodes a ubiquitously expressed protein, hereafter identified as $RPGR^{ex1-19}$, with a predicted molecular mass of approximately 90kD. The first ATG in the transcript that is consistent with translation initiation is located 60 bp downstream from the predicted transcription start site, and the 815 amino acid open reading frame is followed by a 3' untranslated region of 280bp terminating in a polyadenylation signal (25,29). The N-terminal half of the predicted protein, encoded by exons 2-10, contains 6 tandem repeats of 52-54 amino acids, which are highly similar to the conservative RCC1 (regulator of chromosome condensation) protein, the nuclear guanine nucleotide exchange factor for the small GTPase Ran (25,34,35). By catalyzing nucleotide exchange for Ran, RCC1 boasts pivotal roles in regulating nuclear-cytoplasmic transport, mitosis and nuclear-envelope assembly (36). Although there is no evidence of a nuclear localization signal, as is present in the N-terminus of RCC1, there are two possible GTP phosphate binding motifs at residues 13-20 and 30-35 in the predicted $RPGR^{ex1-19}$ peptide. The C-terminal half of $RPGR^{ex1-19}$ contains a domain rich in acidic residues (22% glutamic/aspartic acid and 12% lysine/arginine), and ending in a potential isoprenylation anchorage signal. The functional CaaX isoprenylation motif, where 'a' represents an aliphatic residue and

'X' is leucine, results in proteolytical cleavage of the last three amino acids followed by carboxymethylation of the terminal cysteine, thus providing a means of membrane anchorage (25,37).

Although linkage data analysis suggests that mutations in *XLRP3* are responsible for approximately two-thirds of X-linked RP, initial mutational analysis of *RPGR* found that mutations in the RCC1-homologous domain accounted for only 20-30% of patients with XlRP3. Interestingly, no mutations have been found in exons 16-19 (25,27). Subsequent mutational screening of *XLRP3* revealed that RGPR transcripts undergo tissue specific splicing in the retina by skipping of the splicing donor site of exon 15. Extension of the constitutive exon 15 into intron 15 results in a retina specific group of transcripts that contain exons 1-13 of $RPGR^{ex1-19}$ plus a large, alternatively spliced C-terminal exon, hereafter referred to as open reading frame 15 (ORF15) (26). This exon, deemed a mutational hotspot, contains an extensive, purine-rich region that harbors a high frequency of deletions and insertions, presumably resulting from the repetitive nature of this region. This region, which accounts for the majority of *XLRP3* mutations, encodes a highly repetitive glutamic acid and glycine rich domain of unknown function which is followed by a basic, C-terminal domain (26,28,30).

Functional implications of *XLRP3* mutations

The most clinically severe *XLRP3* mutations are found in exons 1-14 of the *RPGR* locus. These consist of all types of mutations including over 30 identified missense and

nonsense point mutations (26,28,30,38). The identification of at least one mutation, G436D, outside of the RCC1-homologous domain suggests that unknown putative domains between the RCC1-homologous domain and ORF15 maintain a physiological role in the retina (28). Interestingly, four other known mutations within the RCC1-homologous domain (G173R; 786-787delTG; C469+1G>T, intron 5; c.619+9del, intron 6), result in an RP phenotype in addition to a ciliary dyskinesia, such as relapsing otitis media, recurrent upper respiratory tract infractions and hearing loss. Although it is unclear why this small subset of mutations in the RCC1 homologous domain result in a systemic phenotype, this implication nonetheless suggests that RPGR may retain a functional role in tissues outside the retina (39-42).

The majority of missense mutations in the RCC1-homologous domain have been shown to interfere with RPGR function by altering the functional confirmation of the domain thereby reducing or abolishing known protein interactions (43-45). All of the nonsense and frameshift mutations, which include deletions, insertions and duplications, are expected to result in early truncation of the protein. It has been suggested that premature stop codons occurring in exons 2-14 may result in low or absent levels of transcript due to nonsense-mediated decay (46).

Although ORF15 mutations are generally associated with milder disease states (30), the frequency of *XLRP3* mutations found in ORF15 make this unusual exon a prominent focus for study. ORF15 mutations consist mostly of small frame-shift insertions and

deletions with only a few reports of disease-causing transversions (26,28,30). Interestingly, ORF15 can accommodate a variety of in-frame insertions, deletions and residue changes without pathogenic consequences (47). Although it has been hypothesized that ORF15 mutations may result in a series of truncated proteins of varying length, amino acid sequence and charge (46), this hypothesis has not been supported by any experimental data.

Despite phenotypic heterogeneity, there have been some suggested correlations between the location of ORF15 mutations and disease penetrance. Some reports have suggested that mutations toward the 3' end of ORF15 result in a more mild RP phenotype with better retention of rod function or X-linked cone-rod dystrophy while others have suggested that mutations downstream of codon 445 lead to preferential loss of cone function with much less effect on rod function (30-32). There have been numerous reports of a variety of genotype-phenotype associations with ORF15 mutations including X-linked cone-rod dystrophy, cone dystrophy and atrophic macular degeneration and ciliary dyskinesia. ORF15 mutations have also been associated with X-linked dominant forms of RP. These mutations result in phenotype manifestations in both hemizygous males and heterozygous females; however, age of onset is earlier in males (48,49).

Clinical implications

The high prevalence of XLRP3 mutations in RP patients and the genetic heterogeneity of its mutations show that mutational analysis of this locus is of considerable clinical

importance. Although the repetitive nature and high purine content of the ORF15 exon make sequencing difficult, satisfactory mutational analysis methods have fortunately been described (26). This technique will be useful in identifying XLRP3 mutations in carrier testing and prenatal diagnosis, as well as, for clarifying the mode of inheritance (46).

Localization and function of RPGR

RPGR has been shown to localize to the photoreceptor connecting cilia via interaction of its N-terminal RCC1 homology domain to an RPGR-interacting protein, RPGRIP (**Fig. 1.2**) (44,50,51). RPGRIP is a structural component of the ciliary axoneme, and ablation of the *RPGRIP* gene in mice abolishes ciliary localization of RPGR (50,51). In addition to its interaction with RPGRIP, the RCC1 homology domain of RPGR has also been shown to interact with at least 4 other known proteins: phosphodiesterase 6D (PDE6D), a prenyl binding protein; nucleophosmin (NPM), a shuttling protein; and structural maintenance of chromosomes 1A and 3(SMC1/SMC3), two cohesion proteins involved in chromosome and mitotic spindle function (43-45,50,52,53). RPGR is also believed to associate with a number of different axonemal or centrosomal proteins involved in ciliary transport.

Despite the number of known and potential protein-protein interactions, the function of RPGR is not well understood. The presence of an RCC1 homology domain in RPGR and its localization in the connecting cilium suggest that RPGR may regulate

intracellular transport in photoreceptors via an unknown G protein. In mice lacking RPGR, cone photoreceptors exhibit ectopic localization of cone opsin in the cell body and synapse, and both cone and rod photoreceptors degenerate (51). This data is consistent with the proposal that RPGR plays a role in maintaining polarized protein distribution across the connecting cilium by facilitating directional transport or restricting redistribution(54).

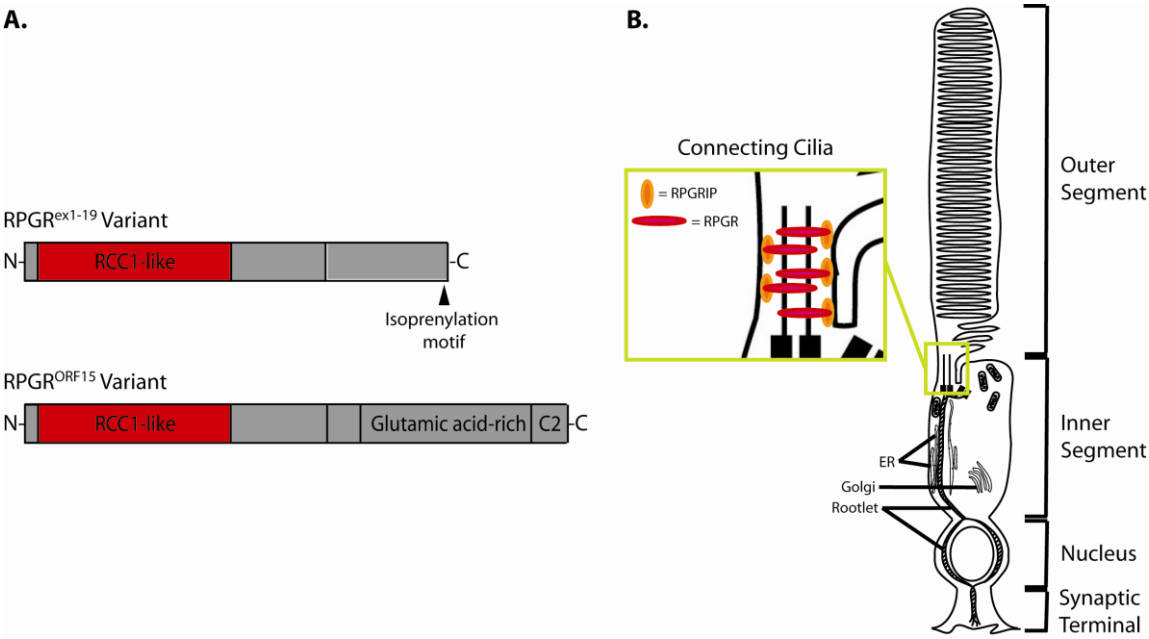

Figure 1.2. Schematic representation of RPGR variants and their anchorage to the photoreceptor connecting cilia. **(A)** Illustration of RPGR protein variants. The RCC-1 homology domain, which binds RPGRIP and is responsible for ciliary localization, is shown in red. **(B)** Schematic representation of a rod photoreceptor illustrating RPGRIP anchorage of RPGR to the connecting cilia.

Furthermore, while the physiological meaning of the presence of multiple RPGR splice variants in photoreceptors is not clear, the conservation of alternative splicing in mammalian retina suggests the importance of this splicing process in photoreceptor

viability. Alternative splicing, which is estimated to modify at least half of all primary mRNA in mammals, greatly increases the coding complexity of the genome by generating a large number of mRNA and protein isoforms from individual genes. Molecular analysis has demonstrated that alternative splicing determines the binding properties, intracellular localization, enzymatic activity, protein stability and posttranslational modifications of a large number of proteins, and is frequently regulated in a developmental or tissue-dependant manner. More than one alternative splice isoforms can be concurrently maintained in the steady state mRNA pool of a single tissue or cell type, and changes in the isoform ratio have been associated with physiological variation and disease susceptibility.

Animal models of XLRP

An RPGR deficient mouse model confirms ciliary localization of Rpgr in photoreceptors, and suggests that ciliary function of Rpgr is facilitative rather than central. In this sense, RPGR may be more appropriately classified as a longevity gene required for the long-term maintenance of photoreceptors (54). Without Rpgr, photoreceptors develop normal morphology and are functional and viable for the first few months of life. Although increased staining of Müller cell processes at 2 months of age is an early indicator of disease progression, photoreceptor cell loss is not evident until 6 months of age with the loss of two rows of nuclei in the outer nuclear layer. Both rod and cone photoreceptors appear susceptible to abnormalities as detected by

electroretinography (ERG) and morphology, though only cone photoreceptors exhibit ectopic localization of opsins in the cell body and synapses.

This model presents a relatively slow retinal phenotype when compared with the observed disease course in human RP3 patients (26,54-57). Such differences in disease progression may be due to different functional consequences between a void in RPGR expression versus expression of mutant RPGR. It has also been suggested that the severity of disease progression in RP3 patients may be dependent on additional genes affecting RPGR expression and/or function (58). This may also be the case in the RPGR-null mouse model, which may be highly dependent on allelic variation and background.

Interestingly, transgenic expression of an ORF15 variant with an in-frame deletion of the purine-rich region in the Rpgr null background results in a significant increase in disease progression. Given that co-expression of the wild-type allele does not rescue the phenotype, this suggests that the mutant ORF15 variant exhibits a dominant, gain-of-function activity (59). A second interesting observation of this model is the retina-specific differential splicing of the purine-rich region of ORF15 exon in photoreceptors versus other cells. This supports the theory that endogenous Rpgr transcripts undergo retina-specific alternative splicing in the purine-rich region (59). However, subsequent rescue of the Rpgr null phenotype by expression of an equivalent, abbreviated ORF15 variant under the control of a different promoter raises questions regarding the dominant

phenotype reported. This latter report nonetheless suggests that a single Rpgr^{ORF15} variant is capable of adequately restoring the loss of Rpgr function in the knockout mouse model and supports the hypothesis that Rpgr^{ORF15} is a functionally significant variant in photoreceptors (60).

An *Rpgrip1* deficient mouse model has also been reported (51). In contrast to the *Rpgr* null model (54), targeted disruption of the *Rpgrip1* locus results in an extremely severe retinal phenotype with early evidence of outer segment morphological dysplasia and disk expansion. These findings are consistent with mutations in the human *RPGRIP1* locus, which are attributed to Leber's congenital amaurosis (LCA), a severe photoreceptor degenerative disorder with appearance of a visual deficit in early childhood (61-63). Loss of ciliary localization of Rpgr in the absence of Rpgrip1, suggests that Rpgrip1 is a stable component of the connecting cilia where it tethers Rpgr. Thus, Rpgr is dependent on Rpgrip1 for subcellular localization and function. As a result, a defect in Rpgrip1 encompasses loss of both Rpgrip and Rpgr function, thus resulting in the more severe clinical phenotype associated with LCA (50,54).

In addition to the described Rpgr mouse models, XLRP studies have also centered around two naturally-occurring canine mutations. Reminiscent of the phenotypic heterogeneity characteristic of human *XLRP3* mutations, mutations in the canine RPGR ortholog, which result in X-linked progressive retinal atrophy 1 and 2 (XLPRA1, XLPRA2), also exhibit contrasting genotype-phenotype correlations (64). A 5-base pair

(bp) deletion in exon ORF15 of XLPRA1 results in a predicted frame-shift and immediate premature stop codon. While these canines show slow degeneration of rod and cone photoreceptors after about 6 months of age, the XLPRA2 canines, which have a 2-bp deletion in exon ORF15 resulting in a premature stop codon 71 amino acids downstream, exhibit a very severe retinal phenotype with abnormal photoreceptor development and rapid degeneration (64). Differential subcellular localization in cultured cells expressing the two allelic variants, shows that while the XLPRA1 ORF15 peptide exhibits the same cytoplasmic subcellular localization of wild-type protein, cells expressing the XLPRA2 mutant allele result in ORF15 colocalization with markers of the endoplasmic reticulum. This data is consistent with observations made in $Rpgr^{ORF15}$ transgenic mice. Together, these results suggest that while many RPGR mutations result in varying degrees of loss-of-function, a subset of ORF15 mutations exhibit a severe gain-of-function phenotype.

Recent identification of two Rpgr orthologs in zebrafish has added zebrafish to the available model systems for RPGR studies (65). Like many zebrafish orthologs of human genes, the two homologous *RPGR* genes reported (*zfrpgr1* and *zfrpgr2*) are probably attributed to a genome duplication that occurred in teleosts. Both genes are expressed in the developing and adult retina as well as more widely during development. Morpholino-induced knockdown of Rpgr expression results in developmental abnormalities similar to those associated with knockdown of other ciliary proteins. Unlike mammals, RPGR knockdown in zebrafish causes developmental abnormalities

including lamination defects, failure to develop photoreceptor outer segments and a small eye phenotype. These defects are rescued by wild-type but not mutant human RPGR alleles. In addition, knockdown of the *zfrpgr2* locus also affects retrograde intracellular transport of organelles. Thus, the authors conclude that *zfrpgr2* is required for normal differentiation and migration of retinal neurons and prevents apoptosis of retinal neurons in zebrafish.

Central hypothesis and specific aims

Based on the published literature, my central hypothesis is that RPGR variants are developmentally regulated and functionally distinct, and that maintenance of the appropriate isoforms is required to coordinately perform essential tasks and maintain normal photoreceptor function.

The experiments presented in the following specific aims are designed to test the above hypothesis in the appropriate in vitro and in vivo experimental models.

Aim I: To analyze RPGR variant expression in the developing retina.

Aim II: To characterize the functional significance of RPGR variants by phenotypic analysis of transgenic mouse models.

Aim III: To further elucidate RPGR function through identification of protein-protein interactions.

The knowledge gained by these studies will significantly advance our understanding of the functional significance of alternative splicing and the pathogenic consequences of RPGR mutations and is a prerequisite for identification of potential therapeutic targets.

CHAPTER II

MISEXPRESSION OF THE CONSTITUTIVE RPGR^{EX1-19} VARIANT LEADS TO SEVERE PHOTORECEPTOR DEGENERATION

Overview

Mutations in the retinitis pigmentosa GTPase regulator (*RPGR*) gene cause of X-linked Retinitis Pigmentosa. The *RPGR* transcript undergoes complex alternative splicing to express both constitutive (Rpgr^{ex1-19}) and Rpgr^{ORF15} variants. Both variants localize to photoreceptor connecting cilia and are believed to play roles in ciliary function. This study examined variability in isoform expression and tested whether the constitutive variant could substitute for Rpgr function in photoreceptors. Rpgr^{ex1-19} and Rpgr^{ORF15} expression during retinal development were compared using immunoblot analysis and immunohistochemistry, and ciliary affinity in adult photoreceptors was assessed by protein fractionation. Transgenic mice expressing either the full-length Rpgr^{ex1-19} or Rpgr^{ORF15} variant were studied using light and electron microscopy and immunofluorescence imaging. The results were compared with those of wild-type and *Rpgr*$^{-/-}$ mice. *Rpgr* expression undergoes dynamic temporal regulation during retinal development and variants exhibit variability for ciliary localization in adult photoreceptors. Transgenic expression of both variants grossly exceeded endogenous *Rpgr* expression in photoreceptors. Although both variants exhibited normal ciliary localization, overexpression of the Rpgr^{ex1-19} variant resulted in atypical accumulation of

Rpgr in photoreceptor outer segments, abnormal photoreceptor morphology and severe retinal degeneration. The Rpgr isoform ratio in the adult retina is critical to photoreceptor integrity. The utilization of distinct Rpgr variants at different stages of photoreceptor maturation suggests independent roles in photoreceptor function. Finally, misexpression of Rpgrex1-19 causes retinal degeneration that is considerably more severe than the Rpgr knockout but photoreceptors tolerate overexpression of RpgrORF15 without evidence of degeneration.

Introduction

X-linked retinitis pigmentosa (XLRP) represents the a severe form of retinitis pigmentosa (RP), a group of inherited retinal dystrophies that result in photoreceptor cell death and the accumulation of intra-retinal pigment-like deposits(25,26). Symptoms include night blindness, progressive loss of peripheral visual fields and eventual loss of central vision(18). Mutations in the *retinitis pigmentosa GTPase regulator* (*RPGR*) gene account for more than 70% of XLRP and approximately 10% of all RP cases(20,25,26). Ablation of the *Rpgr* gene in mice(54) and naturally occurring mutations in dogs(64) also lead to photoreceptor cell degeneration, suggesting that Rpgr is essential for mammalian photoreceptor survival. In addition, both early cone photoreceptor defects and rod degeneration indicate that Rpgr is necessary for the survival of both rods and cones(30,54,66).

Rpgr transcripts undergo a complex splicing process using alternative splicing sites and polyadenylation signals to generate constitutive *Rpgr*$^{ex1-19}$ transcripts and highly variable *Rpgr*^{ORF15} transcripts (**Fig. 2.1**) (26,37,67,68). The Rpgr^{ex1-19} variants are widely expressed and contain exons 1-13 and 16-19, while numerous Rpgr^{ORF15} variants are preferentially expressed in the retina and contain exons 1-13 plus a large, alternatively spliced C-terminal exon 14/15 (26,54). Although both Rpgr^{ex1-19} and Rpgr^{ORF15} localize to the connecting cilia through interaction of their constitutive N-terminal domain with Rpgrip(44,45,50) and evidence suggests that they regulate protein trafficking through the photoreceptor connecting cilia(37,54,69), little is known regarding the physiological significance of expressing two distinct variants.

To further investigate the significance of variable variant expression in photoreceptors, we compared Rpgr^{ex1-19} and Rpgr^{ORF15} expression during retinal development. Using immunoblot analysis and immunofluorescence microscopy, we observed dynamic temporal regulation of Rpgr expression during retinal development. Although Rpgr^{ex1-19} is highly expressed in developing photoreceptors, expression is significantly down-regulated in mature cells. Emergence of the Rpgr^{ORF15} variant, on the other hand, correlates with photoreceptor maturation. By examining transgenic lines expressing only Rpgr^{ex1-19}, we also report that an abundance of Rpgr^{ex1-19} expression in mature photoreceptors results in abnormal accumulation of protein in the outer segments, disruption of outer segment morphology, and rapid retinal degeneration.

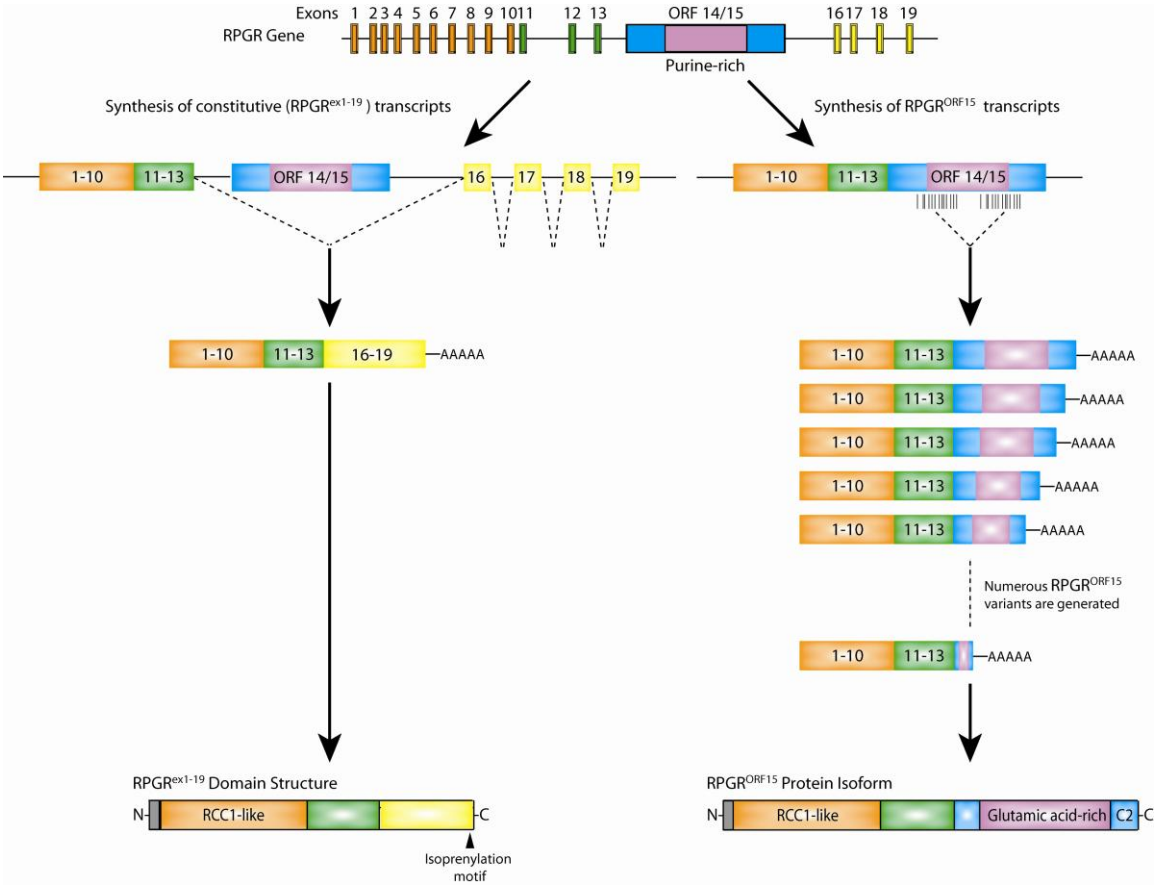

Figure 2.1. Schematic representation of the Rpgr gene structure and illustration of Rpgr expression in the retina. Alternative splicing leads to two groups of *Rpgr* transcripts. *Rpgr*$^{ex1-19}$ includes exons 1-13 and exons 16-19, while *Rpgr*^{ORF15} includes exons 1-13 plus a large, alternatively spliced ORF 14/15. Orange, exons encoding RCC1-like domain common to all Rpgr variants; green, remainder of exons common to all Rpgr variants; yellow, exons 16-19 encoding Rpgr^{ex1-19} specific C-terminal domain, with isoprenylation motif; blue/purple, large exon (ORF 14/15) encoding C-terminal domain of Rpgr^{ORF15}; purple, alternatively spliced region of ORF14/15 encoding glutamic acid-rich domain.

Experimental procedures

Animals

C57BL/6 wild-type mice were obtained from Harlan Laboratories (Houston, TX). The full length *Rpgr*$^{ex1-19}$ was cloned from C57BL/6 wild-type retinal cDNA. Due to variable internal splicing of the ORF14/15 exon present in *Rpgr*^{ORF15} transcripts

(37,67,68), a full-length *Rpgr*^{ORF15} transcript has never, to our knowledge, been successfully cloned. Thus, *Rpgr*^{ORF15} was cloned from a combination of genomic DNA and cDNA. Exons 1-13 were amplified from retinal cDNA and were joined with a full-length, unspliced ORF14/15 exon amplified from genomic DNA. Each clone was introduced into a pCBA vector between the cytomegalovirus (CMV) enhancer β-actin promoter (CBA), which has been shown to drive expression in both rods and cones, and a bovine growth hormone (BGH) polyadenylation sequence. N-terminal 3x-Myc tags were added to distinguish between native and transgenic *Rpgr* expression. Transgenic mice were generated by pronuclear injection of the described transgenic constructs (designated mRDef and mROrf) into C57BL/6 wild-type embryos. Founder mice were bred with C57BL/6 wild-type mice and *Rpgr* $^{-/-}$ mice to generate transgenic mice in a wild-type and *Rpgr* null background, respectively. *Rpgr* $^{-/-}$ littermates were used as a control for assessment of retinal phenotype.

All animals were maintained on a 12-h light – dark cycle, with food and water *ad libitum* and were handled in accordance with the institutional guidelines as approved by the Texas A&M University IACUC (Institutional Animal Care and Use Committee).

Reverse transcription (RT-PCR)

Total RNA was isolated from retina using Trizol reagent (Invitrogen, Carlsbad, CA), and cDNA was generated using the Superscript® One-Step RT-PCR system (Invitrogen, Carlsbad, CA) according to the manufacturer's instructions.

Antibodies

The polyclonal ORF15 antibody was generated in guinea pig and has been previously characterized(69). The other Rpgr antibodies were also previously described (50,69). The locations of the Rpgr antibodies are shown in the antibody map in Figure 2.2A. Green cone opsin antibody (JH492) was provided by Dr. Jeremy Nathans and was used as described (70). Anti-glial fibrillary acidic protein (GFAP) and acetylated α-tubulin (T6793) antibodies were obtained from Sigma Aldrich.

Goat anti-rabbit IgG-horseradish peroxidase conjugate and goat anti-mouse IgG-alkaline phosphatase conjugate (Pierce) were used as secondary antibodies. Alexa fluorochrome-conjugated secondary antibodies for immunostaining were employed (Molecular Probes, Inc).

Immunoblot analyses

Tissues were homogenized in buffer (50mM Tris, pH 7.4, 150mM NaCl, 0.5% NP40) containing a protease inhibitor cocktail (Sigma Aldrich) and were centrifuged at 1000 X g for 2 minutes. For denaturing gel electrophoresis, samples were mixed with 4X SDS sample buffer with β-mercaptoethanol, separated on polyacrylamide gels and then transferred to PVDF membranes (Immobilon-P, Millipore). After blocking the membrane in 5% skim milk in PBS with 0.1% Tween, proteins were detected by applying primary antibody overnight followed by the appropriate secondary antibody for 2 hours. Immunoreactive bands were quantitatively analyzed using Image J

(rsbweb.nih.gov/ij/). Band densities were measured using simple graphical method that involves generating lane profile plots, drawing lines to enclose peaks of interest, and then measuring the peak areas (detailed description of method available at http://rsb.info.nih.gov/ij/docs/menus/analyze.html#gels). As a marker, a Precision Plus Prestained Standard (Biorad), ranging from 10 – 250kD to 25kDa, was used.

Cellular fractionation

Four mouse retinas were dissected and kept on ice or 4°C for the remainder of the procedure, unless otherwise noted. The retinas were homogenized in tissue fractionation buffer (50mm Tris, pH 7.4; 150mm NaCl, and protease inhibitor). The suspension was centrifuged at 500 × *g* for two minutes to remove large debris. The supernatant was centrifuged again at 35,000 × *g* for 30 minutes. The supernatant was transferred to a fresh tube and was designated the cytosolic fraction. The pellet was gently washed in fractionation buffer and was resuspended in NP40 buffer (50mM Tris, pH7.4; 150mM NaCl; 1% Nonidet P-40). After incubating 30 minutes at room temperature, the samples were centrifuged at 35,000 × *g* for 30 minutes. The supernatant was collected and designated as the detergent-soluble fraction. The pellet was carefully washed in NP40 buffer, resuspended in tissue fractionation buffer and designated the axoneme-enriched fraction.

Immunohistochemistry

Unfixed eyes were embedded in optimal cutting temperature (OCT) compound and were snap frozen in liquid nitrogen. Cryosections (10-µm) were cut and collected on pretreated glass slides (Superfrost Plus; Fisher Scientific). Sections were stored at -20°C and used within 2 to 3 days. Immunofluorescence staining was performed as previously described(50,54).

Histology

Eyes were fixed in 4% formaldehyde and were imbedded in optimal cutting temperature (OCT) compound. Histology procedures were carried out as previously described(71).

Dissociated photoreceptors

Dissociated photoreceptor fragments were obtained by mechanical detachment from freshly dissected mouse retinas, as previously described(72). In brief, retinas were suspended in Ringer Solution and were gently homogenized by five passes through a disposable transfer pipette. Cell fragments were allowed to adhere for 5 minutes to pretreated glass slides (Superfrost Plus Microscope Slides; Fisher Scientific). Adhered cell fragments were fixed for 5 minutes in ice-cold methanol, before proceeding with typical immunocytochemical staining as previously described(50,54).

Electron microscopy

After removal of the lens and vitreous, enucleated eyes were fixed in 2% formaldehyde, 2% gluteraldehyde in 0.1M cacodylate buffer. Eyes were washed in 0.1M cacodylate buffer for 3 days and were post-fixed in 1% OsO4 for 1 hour at room temperature. They were then washed once in 0.1M cacodylate buffer and once in water and were gradually dehydrated in 30%, 50%, 70%, 80%, 90% and 95% cold ethanol for 15 minutes each. After warming to room temperature, eyes were incubated in 100% ethanol (15 minutes X 3) followed by propylene oxide (PO). Eyes were infiltrated with 1:2 Epoxy (Epon Araldite with 1.5% DMP-30):PO for 1 hour, 1:1 Epoxy:PO for 1 hour, 3:1 Epoxy:PO for hour and then with 100% Epoxy. After transfer to flat molds, they were heat cured at 65°C for 2 days to polymerize.

Results

Rpgr expression in the developing retina

Since the retina is the only tissue to co-express both $Rpgr^{ex1-19}$ and $Rpgr^{ORF15}$ variants, we examined whether expression of Rpgr variants varied in a temporal manner. We previously showed that Rpgr immunoreactivity is first detectable at the apices of the developing photoreceptor layer at day postnatal day 3 (P3), which correlates with the timing and location of connecting cilia formation(54). To further study the dynamics of Rpgr expression, we compared the expression of $Rpgr^{ex1-19}$ and $Rpgr^{ORF15}$ at specific phases of retinal development. In the mouse, much of retinal development takes place in the three weeks following birth in a process very similar to third-trimester human retinal development (73). Proliferation, migration and differentiation of neuronal precursor

cells in the mouse retina is initiated at embryonic day 12 (E12) and continues through final neuronal differentiation and maturation at approximately P8(74). The final stages of neuronal differentiation and retinal vascular development occur when mice open their eyes and vision is initiated at around P14. Since many factors critical to establishing this visual pathway are regulated during the first two post-natal weeks(75) , we analyzed Rpgr protein levels in retinal homogenates from P3, P7, P14 and adult (2-month) wild-type mice using our anti-S1 antibody (**Fig. 2.2A**), which recognizes both Rpgr variants. $Rpgr^{ex1\text{-}19}$ migrates as a 95-100 kDa band on Western blots. Protein expression was detected at times of neuronal differentiation in the retina and decreased with age, with robust expression at P3 compared to adult expression levels (**Fig. 2.2B**). In contrast, $Rpgr^{ORF15}$ migrates at approximately 200 kDa and the emergence of the $Rpgr^{ORF15}$ variants correlates with the maturation of photoreceptors (**Fig. 2.2B, Fig. 2.3B**). Relative intensities of the $Rpgr^{ex1\text{-}19}$ and $Rpgr^{OFR15}$ bands were quantified using ImageJ software (**Fig. 2.2C**). Thus, our data shows a correlation between changes in the Rpgr isoform ratio and photoreceptor development and maturation.

To compare the localization of Rpgr^{ex1-19} and Rpgr^{ORF15} variants during retinal development, we performed immunohistochemistry on wild-type P3, P7, P14 and adult retinas. Rpgr^{ex1-19} and Rpgr^{ORF15} variants were detected using the anti-S3 and anti-Rpgr ORF15 antibodies, respectively (**Fig. 2.3A; and antibody map, Fig. 2.2A**). In the P3 retina, the Rpgr^{ex1-19} was detected as a narrow band at the apex of the developing photoreceptor layer (**Fig. 2.3A**). The appearance of Rpgr at this time point is consistent with the appearance and location of the emerging photoreceptor connecting cilia (**Fig. 2.3B**). The well-defined band persisted through day 14 but severely diminished in the adult retina. Rpgr^{ORF15} was nearly undetectable until P14 and increased in intensity in the adult retina (**Fig. 2.3A**). This data is consistent with our isoform specific protein level analysis shown in **Figure 2.2B**.

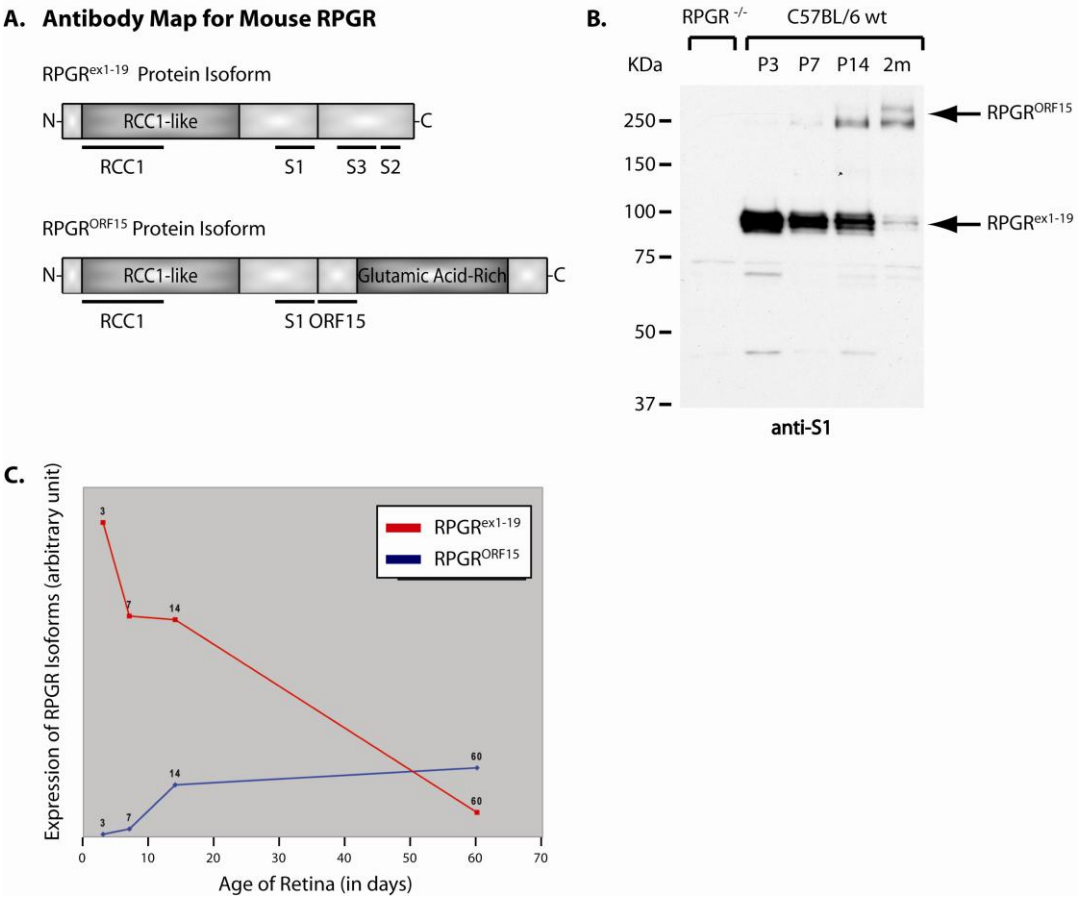

Figure 2.2. Antibody map for mouse Rpgr and comparison of Rpgr^{ex1-19} and Rpgr^{ORF15} expression in the developing retina. (**A**) Top: Illustration of the Rpgr^{ex1-19} variant structure and the location of domains used to generate our RCC1 and S1 polyclonal antibodies, which detect all Rpgr variants, and our S2 and S3, default specific polyclonal antibodies. Bottom: Schematic representation of the Rpgr isoform structure and location of the common domains used to generate polyclonal antibodies against all Rpgr variants (RCC1 and S1) and the ORF15 specific domain used to generate our polyclonal ORF15 antibody. (**B**) Immunoblot analysis of retinal homogenate from wild-type mice at postnatal day 3, 7, 14 and at 2 months. The Rpgr^{ORF15} variants are approximately 250kD and the Rpgr^{ex1-19} variants are roughly 100kD. Retinal homogenate from *Rpgr*$^{-/-}$ mice is shown at left to illustrate antibody specificity. The faint smaller bands detected in the negative control are the result of antibody background and are not detected by any of our other antibodies against Rpgr. (**C**) Graph illustrating relative expression of Rpgr^{ex1-19} and Rpgr^{ORF15} in the developing retina.

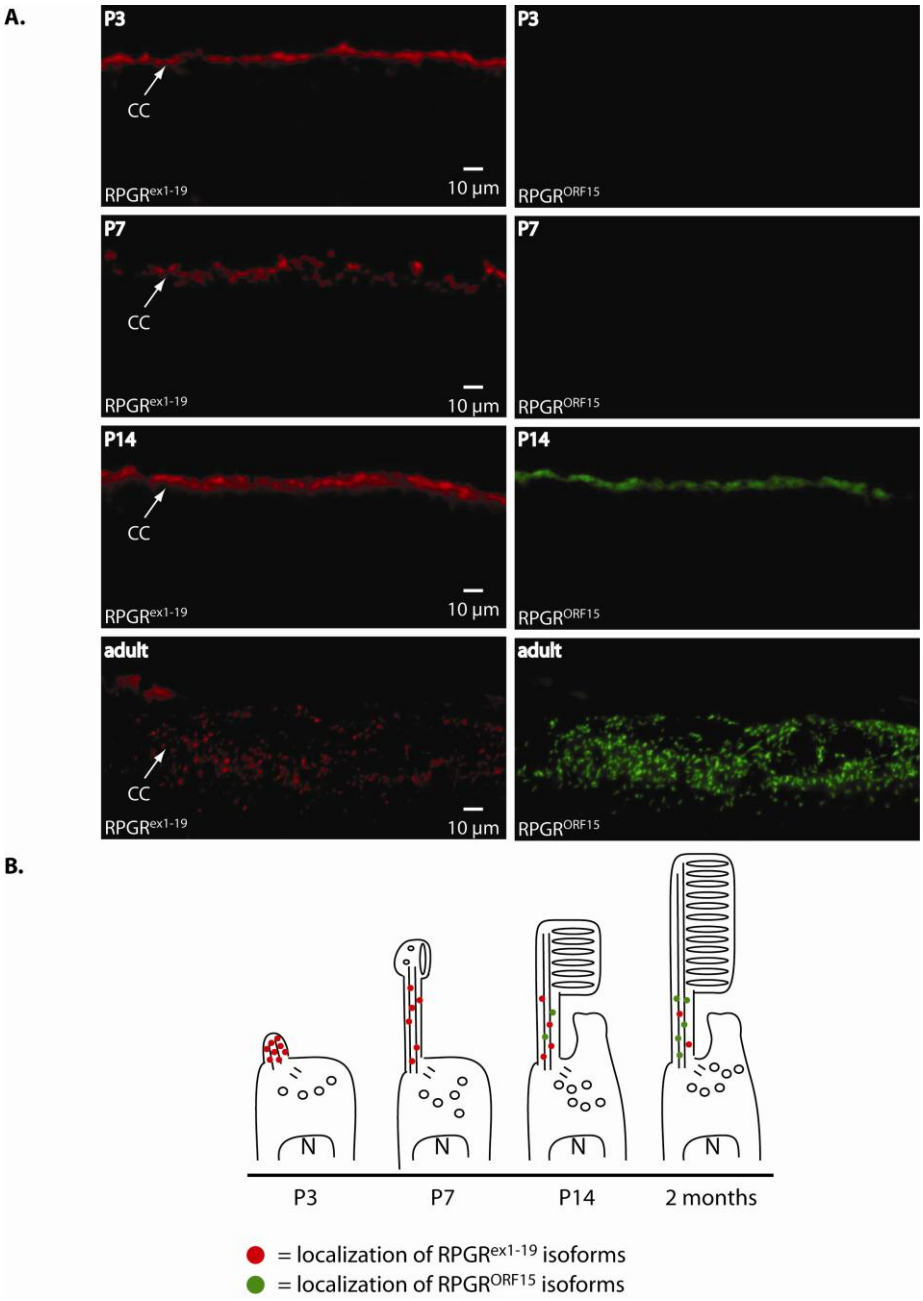

Figure 2.3. Immunohistochemical analysis of Rpgr^{ex1-19} and Rpgr^{ORF15} expression and localization in the developing retina and schematic representation of photoreceptor development at the analyzed time points. **(A)** Double immunostaining of retinal cryosections using our rabbit polyclonal anti-S2 antibody to detect Rpgr^{ex1-19} specific variants (*top*) and our guinea pig polyclonal anti-ORF15 antibody to detect Rpgr^{ORF15} specific variants (*upper middle*). Nuclear staining with DAPI (*lower middle*) and DIC images (*bottom*) are shown to monitor the developmental progression of the retina. **(B)** Illustration representing the development of photoreceptor cells with representative expression and localization of Rpgr^{ex1-19} and Rpgr^{ORF15} variants.

Subcellular distribution of Rpgr variants in retina

The N-terminal domain common to both Rpgr^{ex1-19} and Rpgr^{ORF15} interacts with Rpgrip, a structural component of the ciliary axoneme(50). This interaction anchors Rpgr to the connecting cilia of rod and cone photoreceptors. Upon fractionation of retinal tissue, Rpgr is present in the insoluble, ciliary axoneme enriched fraction in addition to the cytosolic fraction(50). Ciliary localization of all Rpgr variants is lost in Rpgrip null mice, hence eliminating Rpgr from the insoluble fraction (**Fig. 2.4A**).

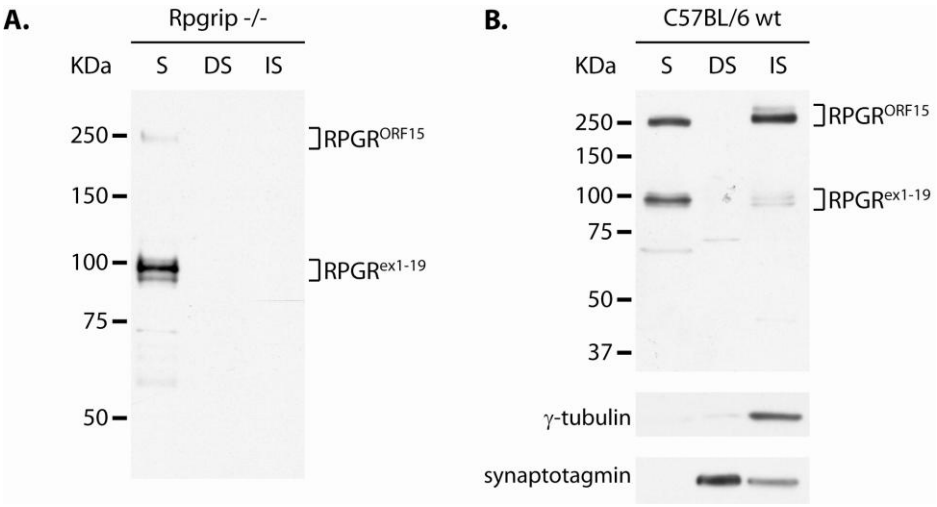

Figure 2.4. Fractionation of retinal homogenate illustrates ciliary localization of Rpgr variants. **(A)** Fractionation of retinal homogenate from Rpgrip $^{-/-}$ retina shows failure of both Rpgr^{ex1-19} and Rpgr^{ORF15} variants to properly localize to the connecting cilia. *S*, soluble protein fraction; *DS*, NP40 detergent soluble fraction; *IS*, NP40 detergent insoluble fraction. **(B)** Immunoblot of fractionated retinal homogenate from C57BL/6 wild-type mice. Rpgr is normally distributed between the soluble fraction (unbound Rpgr) and the NP40 insoluble fraction (Rpgrip bound Rpgr) with a higher proportion of Rpgr^{ORF15} in the NP40 insoluble fraction.

To examine whether both Rpgr variants share equal affinity toward Rpgrip in the connecting cilia, we fractionated retinal homogenates from 2 month old mice. The

cytosolic fraction (soluble, S), the detergent soluble fraction (Nonidet P-40 soluble fraction, DS) and insoluble (IS) fraction were analyzed by immunoblot analysis using our polyclonal anti-S1 antibody (**Fig. 2.4B**). γ-tubulin and synaptotagmin were used as quality controls to insure that the detergent soluble and insoluble fractions were enriched for the membrane bound and ciliary axoneme bound proteins, respectively. Although the amounts of the Rpgr^{ex1-19} and Rpgr^{ORF15} variants in the soluble fraction are approximately equal, a larger percentage of the total Rpgr^{ORF15} isoform population was found in the insoluble fraction. These results indicate that the two groups of variants do not share equal affinity for the ciliary fraction.

Expression of Rpgr^{ex1-19} and Rpgr^{ORF15} in transgenic mice

Rpgr^{ex1-19} and Rpgr^{ORF15} variants both interact with Rpgrip and thus likely share some functional redundancy. However, the discrete C-terminal domains, evidence of developmental differences in isoform expression, and differential binding to the axoneme suggests that the two Rpgr variants also possess independent functions. To investigate the unique role of these two groups of variants in photoreceptor viability, we produced transgenic mice expressing only Rpgr^{ex1-19} or Rpgr^{ORF15}. The mRDef transgenic mice express a full length *Rpgr*$^{ex1-19}$ transcript with an N-terminal 3x Myc tag. This construct (**Fig. 2.5A**) is expressed from a CMV/β-actin promoter (CBA), which drives expression in both rods and cones(60,76)(see Methods). This line was examined in both a wild-type and *Rpgr* null background, herein referred to as mRDef$^{Rpgr\ wt}$ and mRDef$^{Rpgr\ -/-}$, respectively. The mROrf transgenic mice likewise express an *Rpgr*^{ORF15}

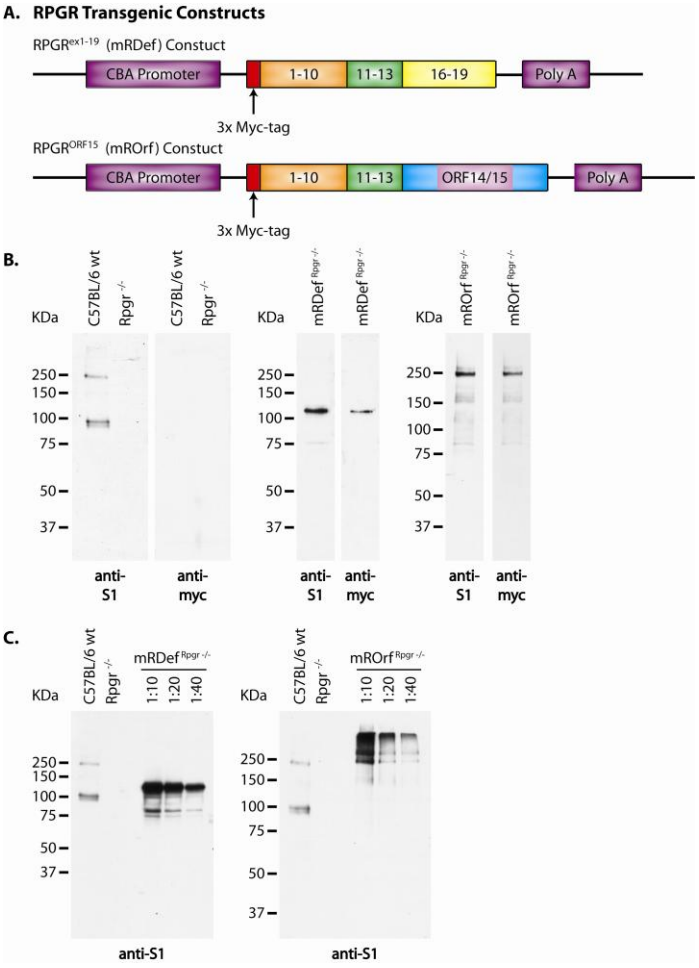

Figure 2.5. Schematic illustration of transgenic constructs and confirmation of transgene expression. **(A)** *Top:* A *Rpgr*$^{ex1-19}$ transcript was cloned between the cytomegalovirus (CMV) enhancer β-actin promoter (CBA) and a bovine growth hormone (BGH) polyadenylation sequence. *Bottom:* A full length *Rpgr*^{ORF15} transcript was cloned from a combination of genomic and cDNA. Exons 1-13 were cloned from wild-type retinal cDNA and the final exon, ORF14/15, was cloned from genomic cDNA. An N-terminal Myc tag was integrated in both transgenic constructs to allow for differentiation between transgenic and native Rpgr expression. **(B)** *Left:* Immunoblot analysis of retinal homogenate from wild-type and *Rpgr*$^{-/-}$ mice using our polyclonal anti-S1 and monoclonal anti-myc antibodies. *Middle:* Verification of transgene expression by immunoblot analysis of retinal homogenate from mRDef$^{Rpgr-/-}$ transgenic mice. *Right:* Verification of transgene expression by immunoblot analysis of retinal homogenate from mROrf$^{Rpgr-/-}$ transgenic mice. **(C)** Comparison transgenic expression levels with Rpgr expression in wild-type retina by immunoblot analysis using the anti-S1 antibody.

construct from a CBA promoter and includes an N-terminal 3x Myc tag (**Fig. 2.5A**). This line was examined in an *Rpgr*$^{-/-}$ background, herein referred to as mROrf $^{Rpgr\ -/-}$.

To confirm that the promoter was driving expression of the transgene in the retina, we analyzed retinal homogenate from mRDef$^{Rpgr\ -/-}$and mROrf $^{Rpgr\ -/-}$transgenic mice by immunoblot analysis. Expression was first confirmed using the S1 antibody followed by a monoclonal anti-myc antibody. An immunoblot of retinal homogenate from wild-type and *Rpgr*$^{-/-}$ mice verified the specificity of our antibodies (**Fig. 2.5B**). The presence of the N-terminal 3X-Myc tag increased the size of the transgenic Rpgr^{ex1-19} protein by an estimated 27kD. Although the transgenic Rpgr^{ORF15} protein has the same N-terminal tag, the increase in size is not evident due to decreased separation of proteins larger than ~250 kDa on the gel.

To estimate the expression level of the transgenic protein, we compared serial dilutions of retinal homogenate from mRDef $^{Rpgr\ -/-}$ and mROrf $^{Rpgr\ -/-}$ transgenic mice with retinal homogenate from wild-type mice (**Fig. 2.5C**). By comparing the 10, 20 and 40 fold dilutions, we estimate there is approximately an 80-fold increase in Rpgr^{ex1-19} expression and about a 40-fold increase in Rpgr^{ORF15} expression in our transgenic mice in comparison to wild-type Rpgr expression levels.

Localization of transgenic Rpgr protein variants

Using immunofluorescence microscopy, we previously determined that Rpgr is concentrated in the connecting cilia of rod and cone photoreceptors(54), as is shown in **Figure 2.6A**. To examine the subcellular localization of transgenic Rpgr proteins, we compared frozen retinal cryosections from mRDef $^{Rpgr\ -/-}$ and mROrf $^{Rpgr\ -/-}$ mice with retinal sections from wild-type mice. All retinal sections were probed with both the S1 antibody and a monoclonal anti-myc antibody (**Fig. 2.6**). Unlike wild-type Rpgr staining, which localizes to the connecting cilium, Rpgr staining in the mRDef $^{Rpgr\ -/-}$ transgenic mice not only labels the connecting cilia but extends into the inner and outer segments (**Fig. 2.6B**). In the mROrf $^{Rpgr\ -/-}$ transgenic mice, Rpgr was observed in the connecting cilia and inner segment but not in the outer segment (**Fig. 2.6C**). This data confirms that both lines express transgenic Rpgr in photoreceptors, and that overexpression of different Rpgr variants results in protein mislocalization. However, only overexpression of Rpgr^{ex1-19} resulted in protein accumulation in the outer segment.

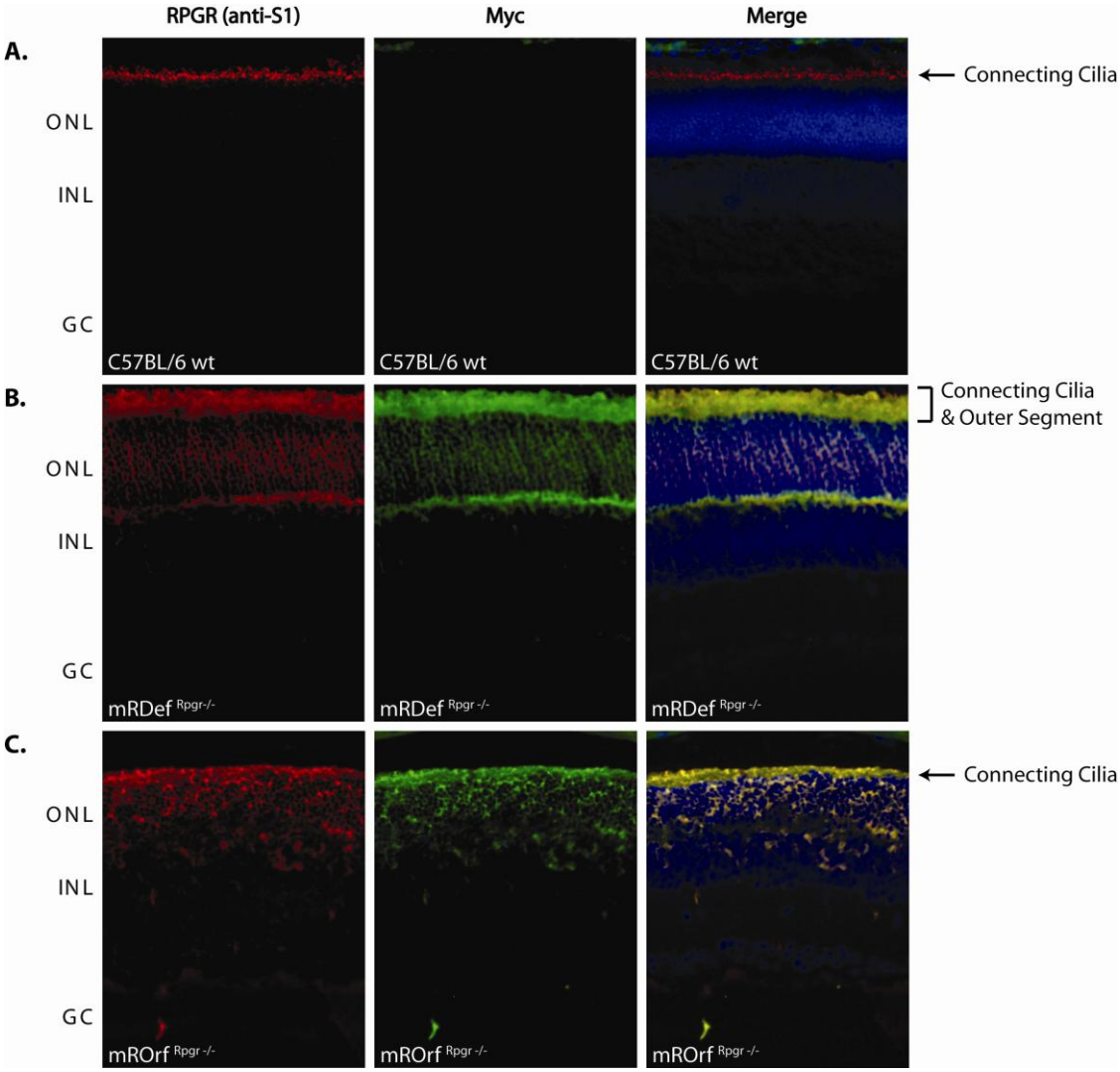

Figure 2.6. Comparison of native Rpgr localization with Rpgr $^{ex1-19}$ and Rpgr ^{ORF15} transgenic expression by immunohistochemical analysis of frozen retinal cryosections. **(A)** Double staining of wild-type retina with our anti-S1 polyclonal antibody (red) and anti-myc monoclonal antibody (green). **(B)** Double staining of transgenic Rpgr^{ex1-19} expression in mRDef $^{Rpgr\ -/-}$ retina with the anti-S1 antibody (red) and anti-myc antibody (green). **(C)** Double staining of transgenic Rpgr ^{ORF15} expression in mROrf $^{Rpgr\ -/-}$ retina with the anti-S1 antibody (red) and anti-myc antibody (green).

To gain better resolution of protein localization, we co-labeled mechanically dissociated photoreceptors for Rpgr and rootletin, a structural component of the inner segment.. These preparations contained mostly shaken-off rod outer segments attached to the connecting cilia with a portion of the inner segments at the proximal end of the connecting cilia. Comparison of the immunofluorescence and DIC images of a wild-type photoreceptor confirms Rpgr localization to the connecting cilium (**Fig. 2.7A**). A schematic diagram of a photoreceptor cell is shown in **Figure 2.7B** to help illustrate the subcellular compartments. The staining pattern of $Rpgr^{ORF15}$ in mROrf $^{Rpgr\ -/-}$ dissociated photoreceptors strongly resembles labeling of Rpgr in wild-type photoreceptors. However, comparison of immunolabeled $Rpgr^{ex1-19}$ in mRDef $^{Rpgr\ -/-}$ photoreceptors shows intense outer segment staining in addition to the normal ciliary staining (**Fig. 2.7A**). This data is consistent with our immunofluorescence staining of retinal sections (**Fig. 2.6**) and confirms that overexpression of $Rpgr^{ex1-19}$ results in an atypical accumulation of protein in the photoreceptor outer segments.

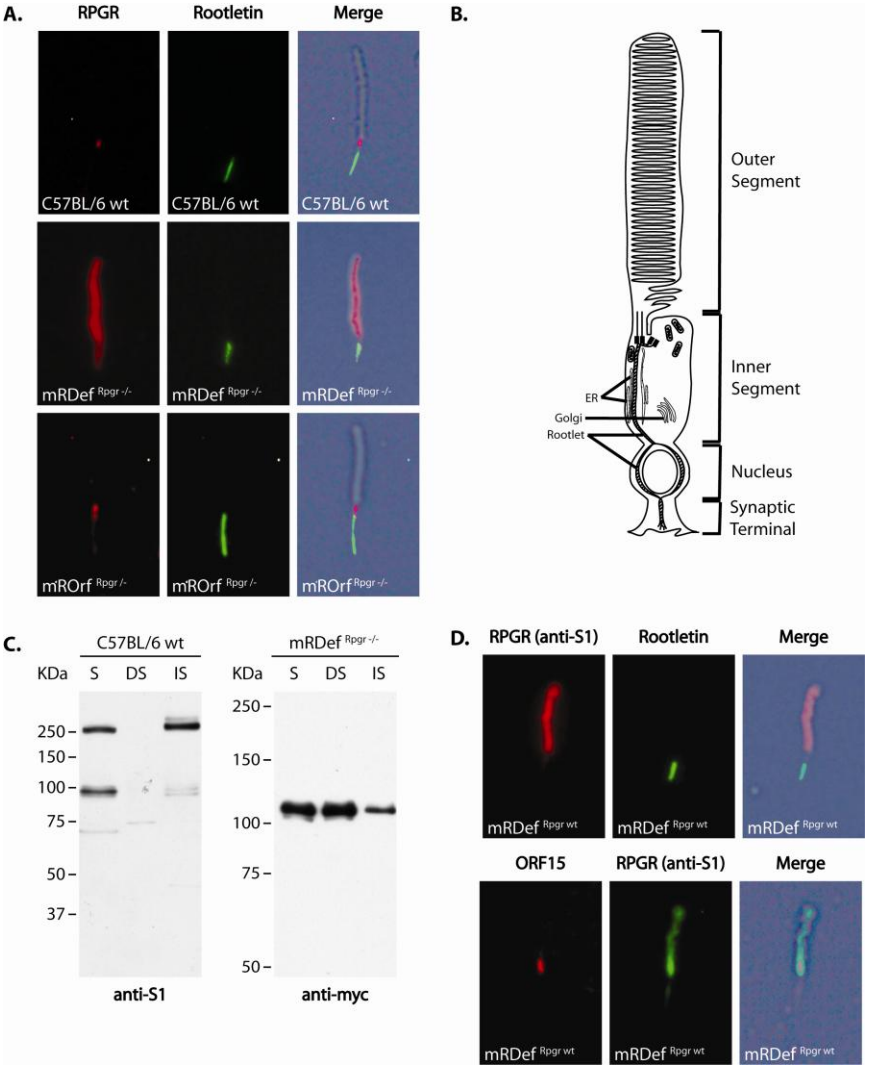

Figure 2.7. Comparison of the subcellular distribution of Rpgr in photoreceptors from wild-type and transgenic retina. **(A)** *Top:* Double staining of a rod photoreceptor from wild-type retina anti-S1 and Rootletin antibody. *Middle:* Double staining of a rod photoreceptor from mRDef $^{Rpgr\ -/-}$ transgenic retina with anti-S1 and Rootletin antibody. *Bottom:* Double staining of a rod photoreceptor from mROrf $^{Rpgr\ -/-}$ transgenic retina with anti-S1 and Rootletin antibody. **(B)** Schematic representation of a rod photoreceptor illustrates subcellular compartments. **(C)** Fractionation of retinal homogenate from wild-type retina and mRDef $^{Rpgr-/-}$ retina shows accumulation of excess Rpgr^{ex1-19} protein in the membrane bound fraction. *S*, soluble protein fraction; *NS*, NP40 detergent soluble fraction; *IS*, NP40 detergent insoluble fraction. *Left:* Immunoblot of fractionated retinal homogenate from wild-type mice. Rpgr is normally distributed between the soluble fraction (unbound Rpgr) and the NP40 insoluble fraction (Rpgrip bound Rpgr). *Right:* Immunoblot of fractionated retinal homogenate from mRDef $^{Rpgr\ -/-}$ mice shows accumulation of default protein in the membrane bound, NP40 soluble fraction. **(D)** Double staining of rod photoreceptors from mRDef transgenic mice in a wild-type background. *Top:* Double staining of all Rpgr variants (anti-S1) and Rootletin (anti-Root6). *Bottom:* Double staining of only the Rpgr ^{ORF15} variants (anti-ORF15) and Rootletin.

The C-terminus of the Rpgr^{ex1-19} peptide contains an isoprenylation signal and is isoprenylated in tissue culture[1, 9, 22]. As isoprenylation often facilitates binding of proteins to target membranes(77,78), we hypothesized that excess Rpgr^{ex1-19} accumulates in the outer segments of mRDef photoreceptors due to interactions with the disc membranes. To test this hypothesis, we compared fractionated retinal homogenate from mRDef $^{Rpgr\ -/-}$ and wild-type mice (**Fig. 2.7C**). In the wild-type retina, Rpgr^{ex1-19} is primarily found in the cytosolic (S) and ciliary axoneme enriched (IS) fractions. In the mRDef retina, there is a moderate increase in the presence of Rpgr^{ex1-19} in both the cytosolic (S) and ciliary axoneme enriched (IS) fractions. However, the most significant change is the accrual of protein in the detergent soluble fraction (NS). Since Nonident P-40 solubilizes membrane-bound proteins, we conclude that Rpgr^{ex1-19} accumulates in the outer segments by interacting with the membranes.

Since Rpgr^{ex1-19} and Rpgr^{ORF15} compete for interaction with Rpgrip in the photoreceptor connecting cilia, we also examine whether an increase in the Rpgr^{ex1-19} concentration disrupts localization of Rpgr^{ORF15} to the connecting cilia. We labeled dissociated photoreceptors from transgenic mRDef mice in a wild-type Rpgr background for all Rpgr variants (anti-S1) and only Rpgr^{ORF15} (anti-ORF15) (**Fig. 2.7D**). Photoreceptors were also labeled with anti-rootletin to confirm the location of subcellular compartments. Despite the overabundance and mislocalization of Rpgr^{ex1-19}, localization of native Rpgr^{ORF15} to the photoreceptor connecting cilia remained unaltered. If Rpgr^{ex1-19} and Rpgr^{ORF15} share equal affinity for Rpgrip, then we would expect the excess

Rpgr^{ex1-19} protein to compete for Rpgrip and diminish the ciliary presence of Rpgr^{ORF15}; however, this was not observed. This is consistent with our earlier findings that a larger proportion of Rpgr^{ORF15} than Rpgr^{ex1-19} is found in the ciliary-enriched fraction (**Fig. 2.4**) and supports our conclusion that Rpgr^{ORF15} has a higher affinity for binding Rpgrip in the connecting cilia.

Retinal disease in Rpgr^{ex1-19} transgenic mice

To evaluate the effects of transgene expression on photoreceptor cell survival, we examined retinal morphology in wild-type mice at 2 months of age and mRDef $^{Rpgr\ -/-}$ mice between 2 and 8 months of age (**Fig. 2.8A-D**). Although the retinal morphology of mRDef $^{Rpgr\ -/-}$ mice was comparable to that of wild-type at the completion of retinal development (P21), retinal cell loss was apparent in young mRDef $^{Rpgr\ -/-}$ retinas. By two months of age, the inner and outer segments of the mRDef $^{Rpgr\ -/-}$ mice were shortened, and a decreased number of nuclei in the outer nuclear layer provided evidence of significant photoreceptor cell loss (**Fig. 2.8B**). Compared to *Rpgr$^{-/-}$* mice (**Fig. 2.8F**), in which retinal cell loss is relatively slow(54), degeneration in mRDef mice was rapid with complete loss of photoreceptors by 8 months (**Fig. 2.8D**). Since the rate of degeneration was similar in both *Rpgr$^{-/-}$* and wild-type backgrounds (**Fig. 2.8D-E**), we conclude that retinal cell loss results from the overexpression of Rpgr^{ex1-19} transgene.

To investigate whether concurrent overexpression of Rpgr^{ORF15} would alter the mRDef transgenic phenotype, we bred mRDef and mROrf mice together in an *Rpgr$^{-/-}$*

background. We compared the retinal morphology of mRDef $^{Rpgr\ -/-,}$ mROrf $^{Rpgr\ -/-}$ and mRDef/mROrf $^{Rpgr\ -/-}$ littermates at 4 months of age (**Fig. 2.8G-I**), and found that the severity of the mRDef transgenic phenotype was unaffected by the presence of Rpgr^{ORF15}. Thus, we conclude that the retinal cell loss in mRDef transgenic mice results in a neomorphic phenotype independent of Rpgr^{ORF15} expression.

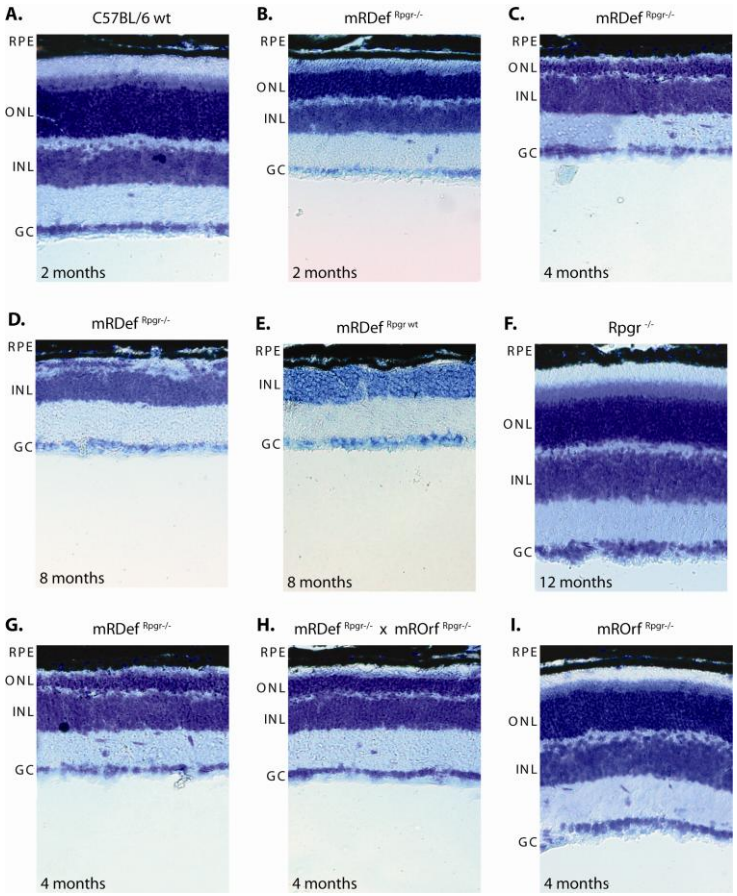

Figure 2.8. Phenotypic analysis of mRDef transgenic mice using light microscopy. **(A-I)** Histological section of wild-type retina at 2 months. RPE, retinal pigment epithelium; ONL, outer nuclear layer; INL, inner nuclear layer; GC, ganglion cell layer. **(B-D)** Histological sections of mRDef$^{Rpgr-/-}$ at 2-8 months of age**. (E**) Histological sections of mRDef$^{Rpgr\ wt}$ at 8 months of age. **(G-I)** mRDef $^{Rpgr\ -/-}$ mice were crossed with mROrf $^{Rpgr\ -/-}$ mice and the retinal phenotypes of 4 month old single and double transgenic littermates were assessed by light microscopy at 4 months of age.

Mislocalization of cone opsins in cone photoreceptor cell bodies and synapses is a prominent phenotype in *Rpgr*$^{-/-}$ mouse retinas before retinal cell loss is even apparent(54). Both blue and green cone opsins, which normally localize in the outer segments, partially mislocalize to the inner segment, perinuclear area, and synaptic regions as early as postnatal day 20 in *Rpgr*$^{-/-}$ mice (data not shown)(54). To observe whether expression of Rpgr^{ex1-19} or Rpgr^{ORF15} rescues the phenotype in cone photoreceptors, we compared mRDef $^{Rpgr\ -/-}$, mROrf $^{Rpgr\ -/-}$ and wild-type control retinas by immunofluorescence for cone opsin (**Fig. 2.9A**). Like *Rpgr*$^{-/-}$ retinas(54), opsins in the mRDef $^{Rpgr\ -/-}$ cone photoreceptors show mislocalization in the inner segment, perinuclear regions and synaptic terminals. In contrast, cone opsin staining in the mROrf $^{Rpgr\ -/-}$ was confined to the cone OS, as in wild type, indicating restoration of Rpgr function in cone cells. Thus, comparison of the number and integrity of cone cells between the two transgenic mice demonstrates that Rpgr^{ORF15} but not Rpgr^{ex1-19} is able to rescue the *Rpgr*$^{-/-}$ phenotype.

Upregulation of glial fibrillary acidic protein (GFAP) expression in the retina is a nonspecific marker of retinal degeneration. In *Rpgr*$^{-/-}$ retinas, GFAP upregulation indicates degenerative changes prior to retinal cell loss(54). As an additional outcome measure for the mRDef $^{Rpgr\ -/-}$ and mROrf $^{Rpgr\ -/-}$ transgenic phenotypes, we examined GFAP expression in transgenic and control animals (**Fig. 2.9B**). As expected, GFAP was clearly unregulated in the mRDef $^{Rpgr\ -/-}$ mice with expansion of staining into the

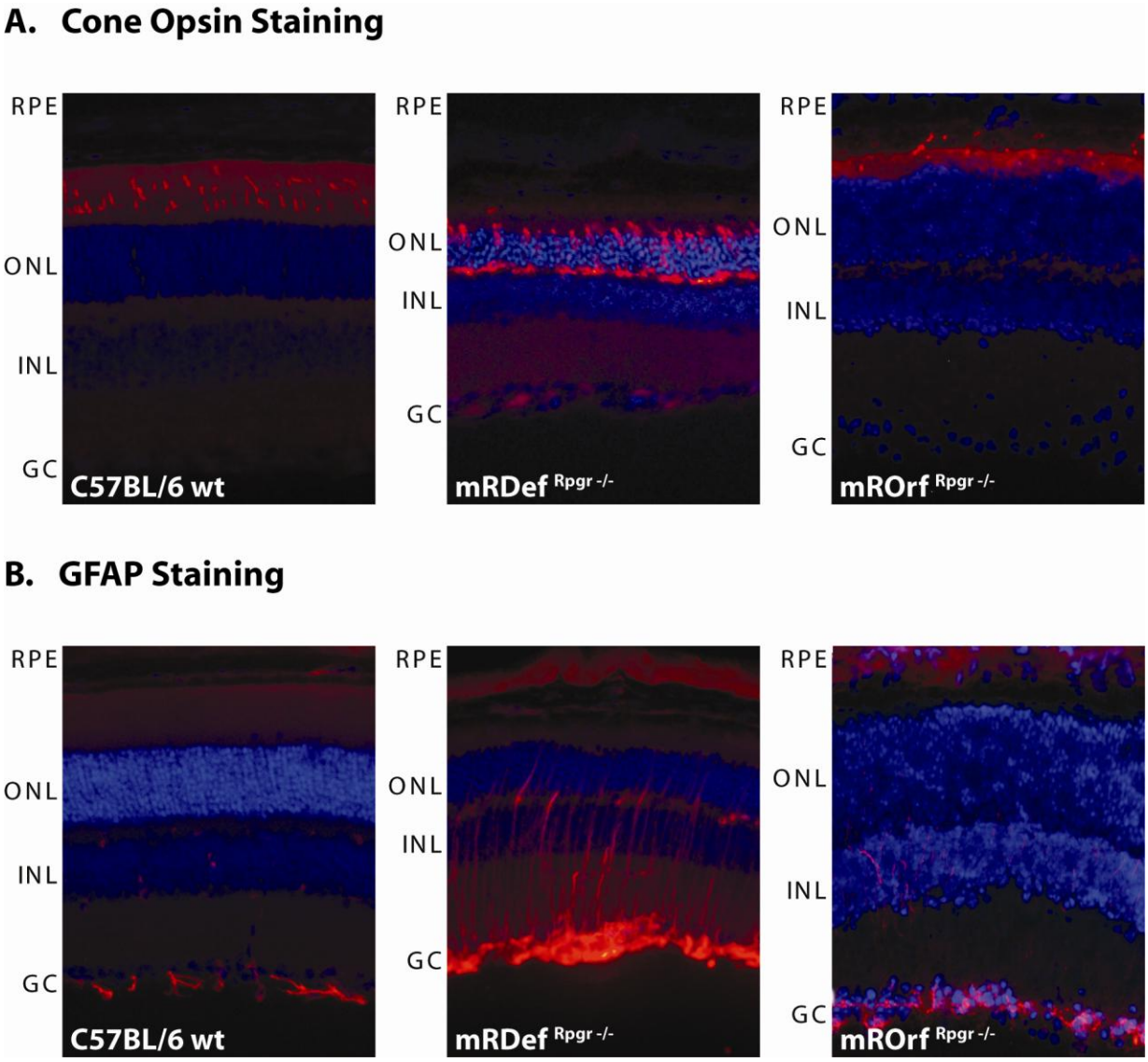

Figure 2.9. Mislocalization of opsins and up-regulation of GFAP in mRDef transgenic mice. **(A-B)** RPE, retinal pigment epithelium; ONL, outer nuclear layer; INL, inner nuclear layer; GC, ganglion cell layer. **(A)** Immunohistochemical analysis of opsin localization in retinal cryosections using green cone opsin specific antibody. *Left:* wild-type retina; *Middle:* mRDef $^{Rpgr\ -/-}$ transgenic retina; *Right:* mROrf $^{Rpgr\ -/-}$ transgenic retina **(B)** Upregulation of GFAP immunoreactivity in mRDef $^{Rpgr\ -/-}$ retina. *Left:* wild-type retina; *Middle:* mRDef $^{Rpgr\ -/-}$ transgenic retina; *Right:* mROrf $^{Rpgr\ -/-}$ transgenic retina.

outer retina. Virtually no GFAP signal was detected in the wild-type and mROrf $^{Rpgr\ -/-}$ retinas.

Because of the rate of degenerative changes and the aforementioned accumulation of $Rpgr^{ex1-19}$ protein in the outer segments of mRDef $^{Rpgr\ -/-}$ transgenic mice, photoreceptor outer segment morphology was assessed by electron microscopy at 2 months of age **Fig. 2.10**). The outer segments were notably disorganized in the transgenic mice with disruption of the conventional parallel arrangement of disk membranes and poorly defined outer segment morphologies. Perimeters were undefined and disk diameters to the long axis of the outer segments instead of the normal perpendicular orientation. Although such defects are not seen in the $Rpgr^{-/-}$ mice, these observations are reminiscent of the abnormal disk morphology seen in the $Rpgrip^{-/-}$ mice(51).

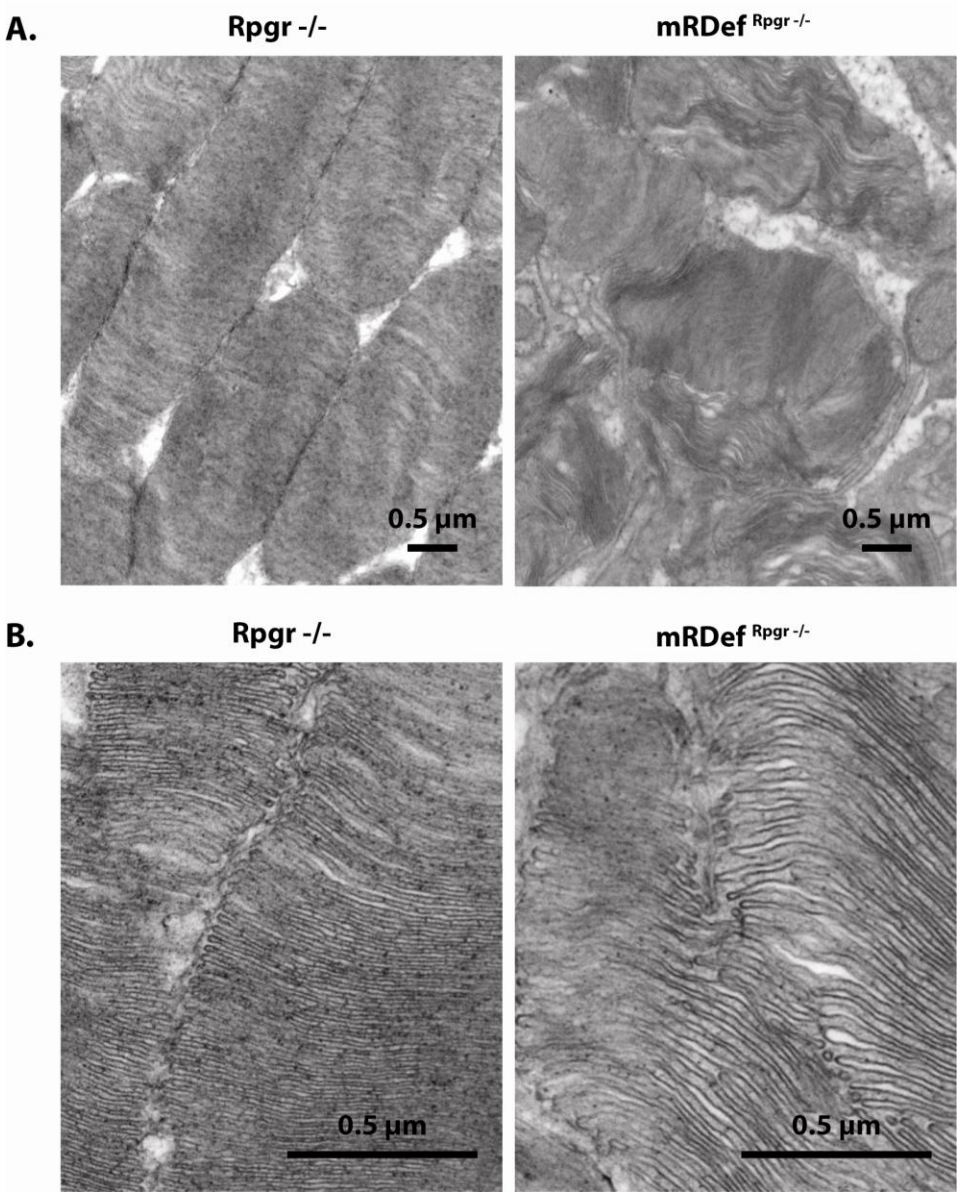

Figure 2.10. Ultrastructural examination of photoreceptor outer segments in mRDef transgenic mice. **(A)** Digital TEM images at 11,000X. *Left:* TEM image of photoreceptor outer segments in two month old *Rpgr* $^{-/-}$ retina. *Right:* TEM image of photoreceptor outer segments in two month old mRDef $^{Rpgr\ -/-}$ retina. **(B)** Digital TEM images at 44,000X. *Left:* TEM image of photoreceptor outer segments in two month old *Rpgr* $^{-/-}$ retina. *Right:* TEM image of photoreceptor outer segments in two month old mRDef $^{Rpgr\ -/-}$ retina.

Discussion

An important finding of this work is the differential regulation of Rpgr variant expression during photoreceptor development. Although previous analyses of mice lacking Rpgr indicated that Rpgr is not essential for mammalian photoreceptor development(54), the robust expression of the $Rpgr^{ex1-19}$ variant during retinal development is nonetheless suggestive of a functional role in cellular development. These conclusions are consistent with a recent report identifying two Rpgr orthologs in zebrafish, which were also reported to have more widespread expression during development. Like many zebrafish orthologs of human genes, the two homologous *RPGR* genes reported (*zfrpgr1* and *zfrpgr2*) are probably attributed to a genome duplication that occurred in teleosts. Unlike mammals, Rpgr knockdown in zebrafish results in developmental abnormalities, including failure to develop photoreceptor outer segments(65), suggesting that Rpgr is required for normal retinal development. In addition, our data also indicates that emergence of the $Rpgr^{ORF15}$ variants follows a reciprocal expression pattern, coinciding with photoreceptor maturation. This supports the idea that $Rpgr^{ORF15}$ plays a physiological role in the integrity of mature photoreceptors. While it has been speculated that $Rpgr^{ORF15}$ is the functionally significant variant in photoreceptors(60), the dynamics of Rpgr expression in emerging photoreceptors suggests that both the $Rpgr^{ORF15}$ and $Rpgr^{ex1-19}$ variants retain some independent, isoform specific functions.

In this study, we also address whether the Rpgr^{ex1-19} variant alone is able to restore function to photoreceptors lacking endogenous Rpgr. Photoreceptors in Rpgr^{ex1-19} transgenic mice exhibit atypical accumulation and interaction of Rpgr^{ex1-19} protein with the membranous outer segments, severe histopathological changes in the photoreceptor outer segments, mislocalization of cone opsin and up regulation of GFAP. Expression of the Rpgr^{ex1-19} transgene results in a substantially more severe phenotype than that of the previously reported *Rpgr*$^{-/-}$ mice(54) with photoreceptor degeneration apparent from an early age.

Rpgr^{ex1-19} expression in our transgenic mice exceeds wild-type endogenous Rpgr^{ex1-19} expression by several fold. Thus, the observed phenotype may be a non-specific consequence associated with the intense level of overexpression. However, since similar overexpression of the Rpgr^{ORF15} variant did not result in atypical accumulation of protein in the outer segment nor a degenerative retinal phenotype, we conclude that our report describes an Rpgr^{ex1-19} specific phenomenon. Although endogenous Rpgr^{ex1-19} expression in adult photoreceptors is minimal, further investigation of this acquired function, may nonetheless provide evidence of native Rpgr^{ex1-19} function in developing and/or mature photoreceptors.

The Rpgr^{ex1-19} variant differs from the Rpgr^{ORF15} variant by the presence of a C-terminal isoprenylation motif (25,37,46,79). By immunofluorescence, we observe that excess Rpgr^{ex1-19} protein accumulates in photoreceptor outer segments. Such mislocalized

accumulation is likely related to the membranous nature of the outer segment structure and the inherent properties of the isoprenylation signal. In general, isoprenylation motifs signal the addition of prenyl groups at carboxy-terminal cysteine residues. The functional consequence of such posttranslational protein modification is anchorage of prenylated proteins to cell membranes(77,78).

Given evidence of severely diminished $Rpgr^{ex1-19}$ expression in mature photoreceptors and the affinity of $Rpgr^{ex1-19}$ to tightly bind Rpgrip in the connecting cilia(44,45,50), the presence of Rpgrip is likely sufficient to limit localization of endogenous Rpgr to the connecting cilia in mature photoreceptors. This would suggest that if the concentration of $Rpgr^{ex1-19}$ exceeds the binding capacity of Rpgrip or if binding is otherwise interrupted, default may begin to mislocalize and accumulate in the photoreceptor outer segments. By electron microscopy, it is clear that this accumulation of protein both functionally and morphologically disrupts the organized structure of the outer segments' membranous disks. In addition, isoprenylation of Rpgr may be required for some form of ciliary trafficking during very early stages of photoreceptor development before the appearance of the outer segments. Thus, the $Rpgr^{ex1-19}$ variants may possess different functions during early development as compared to the function of $Rpgr^{ORF15}$ following ciliogenesis and outer segment maturation.

Although we have previously shown that expression of a single $Rpgr^{ORF15}$ variant substantially rescues the *Rpgr* knockout phenotype(60) , these more recent findings

should also be taken into consideration when designing therapeutic treatment for *RPGR* patients. Unfortunately, there is a void in knowledge regarding protein expression in *RPGR* patients. Although a majority of *RPGR* mutations are in the ORF15 exon and thus only directly affect the integrity of the $Rpgr^{ORF15}$ variants, there is some possibility of indirect effects on $Rpgr^{ex1-19}$ expression as well. Given that all *RPGR* variants are under the control of a single promoter there exists some possibility that $Rpgr^{ex1-19}$ expression may be affected by endogenous attempts to compensate for the loss of functional $Rpgr^{ORF15}$. This theory may explain some of the variability associated with human genotype-phenotype correlation, as well as, the surprisingly mild phenotype of *Rpgr* null mouse models when compared with XlRP3-affected humans and dogs. Furthermore, if this theory is upheld, then introduction of the $Rpgr^{ORF15}$ variant by gene therapy also has the potential to affect endogenous Rpgr expression. In either case, up-regulation of $Rpgr^{ex1-19}$ expression has the potential to be more detrimental to photoreceptor integrity and disease progression than the lack of functional $Rpgr^{ORF15}$.

CHAPTER III

RPGR^{ORF15} CONNECTS TO THE USHER PROTEIN NETWORK THROUGH DIRECT INTERACTIONS WITH MULTIPLE WHIRLIN ISOFORMS

Overview

Mutations in the *retinitis pigmentosa GTPase regulator (RPGR)* gene account for more than 70% of the cases of X-linked Retinitis Pigmentosa. RPGR undergoes complex alternative splicing to express both constitutive and ORF15 variants, and the latter have been reported to be functionally significant in the maintenance of photoreceptor viability. While functional studies of RPGR suggest a role in intracellular protein trafficking across the connecting cilia, the function of RPGR is not well understood and little is known about functional binding partners. In this study, we show that the C-terminus of RPGR^{ORF15} binds whirlin, a PDZ-domain scaffold protein and known member of the Usher protein network. RPGR^{ORF15}-whirlin interaction was confirmed using *in vitro* binding assays and co-immunoprecipitation from retinal tissue, and both proteins were shown to co-localize in the photoreceptor connecting cilia *in vivo*. Our data also demonstrate that whirlin expresses multiple isoforms in photoreceptors with variable subcellular localization. Whirlin expression has previously been reported in photoreceptors and cochlear hair cells, and mutations in whirlin cause Usher syndrome (USH2D) and non-syndromic congenital deafness (DFNB31). Since mutations in the 5'-end of whirlin are associated with the syndromic phenotype associated with USH2D, the

identification of novel N-terminal isoforms in the retina and a novel RPGR^{ORF15}-whirlin interaction provide a potential mechanism for the retinal phenotype observed in USH2D.

Introduction

X-linked retinitis pigmentosa (XLRP) represents the most severe class of Retinitis Pigmentosa (RP), a group of inherited diseases causing progressive retinal degeneration (25,26). RP is characterized by night blindness, progressive loss of visual fields, and eventual blindness, all of which result from photoreceptor cell death and accumulation of intra-retinal pigment-like deposits (18). Mutations in the *retinitis pigmentosa GTPase regulator* (*RPGR*) gene account for more than 70% of XLRP and approximately 10% of all RP cases (20,25,26). Ablation of the *Rpgr* gene in mice (54) and naturally occurring mutations in dogs (64) also cause photoreceptor cell degeneration, suggesting that photoreceptor survival requires RPGR. In addition, evidence of early cone photoreceptor defects indicates that RPGR is necessary for the survival of both types of photoreceptors (30,54,66).

RPGR transcripts undergo complex alternative splicing to generate default and RPGR^{ORF15} transcripts (26,37,67,68) (**Fig. 3.1A-B**). Default variants are widely expressed and contain nineteen exons (RPGR $^{ex1-19}$), while the RPGR^{ORF15} variants are preferentially expressed in the retina and contain exons 1-13 plus a large, alternatively spliced C-terminal exon 14/15 (26,54). Both variants share a common N-terminal domain, however, their remaining C-terminal domains vary considerably (25,26,54).

The presence of disease-causing mutations within the ORF15 exon suggests that $RPGR^{ORF15}$ variants are functionally significant (26).

RPGR localizes to the photoreceptor connecting cilium (37,52,54). One of the primary defects in mice lacking RPGR is cone opsin mislocalization in photoreceptors (54). Although this suggests that RPGR regulates protein trafficking through the connecting cilia, the function of RPGR is poorly understood and little is known about physiological binding partners.

To further investigate the *in vivo* function of RPGR, we used a yeast two-hybrid screen to identify potential interacting partners of $RPGR^{ORF15}$. We identified a novel N-terminal variant of whirlin, a putative PDZ scaffold protein expressed in cochlear hair cells and retinal photoreceptors. Whirlin is a member of the Usher protein network, a dynamic complex which includes motor proteins, scaffold proteins, cell adhesion molecules and transmembrane receptors critical for development and maintenance of these sensorineural cells (80-86). Mutations in the *DFNB31/WHRN* gene encoding whirlin cause the non-syndromic deafness DFNB31 and Usher Syndrome, Type 2D (USH2D), an autosomal recessive condition characterized by congenital deafness and RP (87,88). The direct association between whirlin and $RPGR^{ORF15}$ provides a novel mechanism for RP in USH2D.

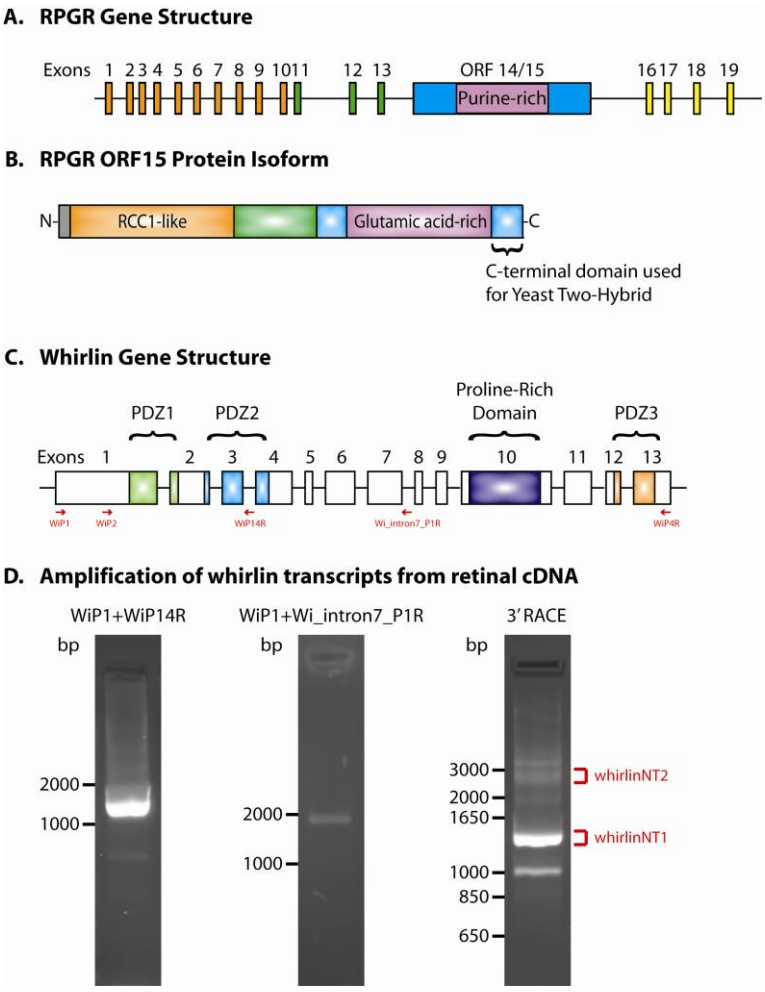

Figure 3.1. Illustration of the RPGR and whirlin/DFNB31 gene structures and analysis of whirlin expression in the mouse retina at the RNA level. (A) Schematic representation of the *RPGR* gene structure. Alternative splicing leads to two groups of RPGR transcripts; RPGR default includes exons 1-13 and exons 16-19 while RPGR^{ORF15} includes exons 1-13 plus a large, alternatively spliced ORF 14/15. *Orange*, exons encoding RCC1-like domain common to all RPGR isoforms; *green*, remainder of exons common to all RPGR isoforms; *blue/purple*, exon (ORF 14/15) unique to RPGR^{ORF15}; *purple*, alternatively spliced region of ORF14/15 encoding glutamic acid-rich domain. (B) Illustration of the RPGR^{ORF15} isoform. All colors correspond to their respective exons in shown Fig. 1A. Brackets indicate the location of domain used as bait in the yeast two-hybrid screen. (C) Schematic representation of the *whirlin/DFNB31* gene structure. Whirlin is composed of 13 exons encoding three PDZ domains and a proline-rich region. Exons and encoded domains are drawn approximately to scale. PCR primers used for amplification of whirlin transcripts are shown as red arrows. (D) Amplification of whirlin N-terminal transcripts from C57BL/6 retinal cDNA. L*eft/Center*: Whirlin mRNA transcripts were reverse transcribed and amplified using primers shown in Fig. 2A. The whirlinNT1 transcript, which includes intron 3, was amplified by WiP1 and WiP14R, and the whirlinNT2 transcript, which includes intron 7, was amplified by WiP1 and Wi_intron7_P1R. *Right*: Whirlin N-terminal transcripts were also amplified by nested PCR of 3'RACE retinal cDNA. Transcripts were first amplified using WiP1 and GeneRacer 3' Primer followed by WiP2 and GeneRacer 3' Nested Primer. The regions excised and used to clone and sequence the whirlinNT1 and whirlinNT2 transcripts are indicated by the red brackets.

Experimental procedures

Animals

C57BL/6 mice were obtained from Harlan Laboratories (Houston, TX) and the RPGRIP knockout mice were generated by targeted disruption of the *RPGRIP* gene as previously described (51). All animals were maintained on a 12-h light – dark cycle, with food and water *ad libitum* and were handled in accordance with the institutional guidelines as approved by the Texas A&M University IACUC (Institutional Animal Care and Use Committee). Whirlin knockout retina were a gift from Jun Yang, (Moran Eye Center, Salt Lake City, Utah).

Yeast two-hybrid analysis

Yeast two-hybrid screening was performed using the GAL4-based two-hybrid system. Cloning vectors, yeast host cells and reagents were purchased from CLONTECH Laboratory (Palo Alto, CA). A retinal cDNA library was constructed from poly(A)+ RNA from C57BL/6 mouse retinas, and the cDNAs were inserted into the pACT2 plasmid vector downstream from the GAL4 activation domain. The bait plasmid was constructed by inserting a cDNA encoding the bait protein into the pGBKT7 plasmid vector downstream from the GAL4 DNA binding domain. The bait protein consisted of the C-terminus of mouse $RPGR^{ORF15}$ (amino acids 679-781). Reference to the numbering of exon ORF15 of the $RPGR^{ORF15}$ sequence in this report is based on GenBank accession, HQ260316. A sequential transformation protocol was used to introduce bait and library plasmids into yeast. Yeast AH109 cells were first transformed

with the bait plasmid, and the bait protein expression was verified by immunoblot. Competent cells were then prepared from a yeast clone harboring the bait plasmid and transformed with the library plasmids. Positive colonies were isolated based on their ability to express nutritional markers HIS3 and ADE2 and the lacZ reporter, driven by different Gal4-responsive promoters to minimize false positives due to fortuitous activation of a particular promoter. Candidate plasmids were sequenced on an ABI 3100 Automated Sequencer.

Reverse transcription-polymerase chain reaction (RT-PCR)

Total RNA was prepared from mouse retina using TRIzol reagent (Invitrogen), and RT-PCR was performed using the SuperScript III RT-PCR kit (Invitrogen) according to the manufacturer's instructions. PCR reactions were performed with PfuUltra II Fusion HS DNA Polymerase (Stratagene). WiP1 (5'-ATGAACGCACAGCTGGACGGC-3') and WiP4R (5'-CTGATAGCCCTGAACTTGGCC-3') primers were used to amplify the full length whirlin transcript. WiP1 and WiP14R (5'-CAGTAGTTGCATCAAAACATTAGCTGCC-3') primers were used to amplify the whirlin NT1 transcript. WiP1 and Wi_intron7_P1R primers were used to amplify the whirlin NT2 transcript. The locations of all primers are illustrated in **Fig. 3.1C**. PCR products were gel purified and cloned using the StrataClone Ultra Blunt PCR Cloning Kit (Stratagene).

3' rapid amplification of cDNA ends

Total RNA was prepared from mouse retina using TRI reagent (Sigma Aldrich). RT-PCR was performed using the Generacer™ Kit purchased (Invitrogen) as per the manufacturer's instructions. Whirlin transcripts were amplified by nested PCR using whirlin specific 5' primers (WiP1 and WiP2, 5'-AGCTGCTCTTGCACCAGTACACG-3') and the GeneRacer 3' Primer and GeneRacer 3' Nested Primer. For cloning, 3' RACE products were gel purified and ligated using the Zero Blunt® TOPO® PCR cloning kit (Invitrogen).

Cell culture and transfection

AAV293 cells were maintained in Dulbecco's modified Eagle medium (DMEM) supplemented with 5% fetal bovine serum, penicillin (100 U/ml) and streptomycin (130ug/ml) at 37°C in an atmosphere of 5% CO_2. Transient transfection was performed using the standard calcium phosphate method. Transfected cells were washed once with PBS and were homogenized in 50mM Tris, pH 7.4, 150mM NaCl, 0.5% NP40. The cell lysates were cleared by centrifugation at 12,000 X *g* for 10 minutes, and the supernatants were used for subsequent immunoblot analysis or protein pull-down assays.

Protein pull-down assays

N-terminal MBP fusion proteins containing either the WhirlinNT1 variant (GenBank accession, HQ148552), the whirlin PDZ_1 domain (amino acids 141-216; GenBank accession, NP_082916.1), the whirlin PDZ_2 domain (amino acids 270-350), the region

between the two PDZ domains (amino acids 217-269), or MBP alone were expressed in *Escherichia coli* Rosetta cells using the pMALC2X expression vector (New England Biolabs). To verify that equivalent amounts of the specific MBP-fusion proteins and MBP protein alone were used, purified protein was analyzed by Bradford assay and equal molar concentrations were calculated. A single $RPGR^{ORF15}$ transcript was obtained by RT-PCR using ORF15 specific primers and cloned using the Zero Blunt® TOPO® PCR cloning kit (Invitrogen). After subcloning into a mammalian expression vector under the control of the CBA (CMV enhancer/chicken β-actin) promoter, the 75kD isoform was expressed by transient transfection in HEK293 cells. Increasing equimolar concentrations (0.625 mM, 1.875 mM, and 5.625 mM) of the MBP fusion proteins and MBP protein alone were immobilized on amylose resin and were incubated with HEK293 cell lysate expressing the 75kD $RPGR^{ORF15}$ variant for 2 hours at room temperature with gentle rocking. The beads were washed four times with binding buffer, resuspended as above and assayed using anti-S1 antibody.

The C-terminal domain of mouse $RPGR^{ORF15}$ (amino acids 679-781 of exon 14/15), which was used as bait in the yeast two-hybrid screen, was cloned into the pMALC2X expression vector (Invitrogen). An N-terminal maltose binding protein fusion containing the ORF15 C-terminal domain and MBP alone were expressed in Rosetta *Escherichia coli* cells and purified. Purified protein was quantified using a Bradford assay and equivalent molar concentrations were calculated. cDNAs for expression of the whirlinNT1 and long whirlin isoforms were obtained by RT-PCR as described, and were

subcloned into pcDNA3.1(+)/3xMyc mammalian expression vector. The full length whirlin and whirlinNT1 variants were expressed in HEK293 cells, and extracts were equalized by immunoblot analysis with anti-myc tag antibody. Purified MBP fusion protein of increasing molar concentration (0.625 mM, 1.875 mM, and 5.625 mM) were immobilized on amylose resin and were incubated with equal amounts of full length whirlin and whirlinNT1 for 2 hours at room temperature with gentle rocking. Purified MBP alone was used at the highest equimolar concentration (5.625mM) as a negative control. The beads were washed four times with binding buffer (25mM Tris, pH 7.4; 100mM NaCl; 1mM $MgCl_2$; 0.1% NP40). Bound proteins were resuspended in 30µl of 2X SDS sample buffer with β-mercaptoethanol and analyzed by immunoblot analysis using anti-myc tag antibody.

Co-immunoprecipitation

Retinal homogenate from six week old RPGRIP knockout mice was incubated overnight at 4°C with either anti-S1 antibody or pre-inoculated rabbit serum. The antibody-protein complex was immobilized on Dynabeads® Protein G (Invitrogen) following the manufacturer's instructions. Co-immunoprecipitated protein was visualized by immunoblot using whirlin-specific primary antibody, which was conjugated to alkaline phosphatase for direct detection by chemiluminescence without subsequent incubation with a secondary antibody.

Antibodies

Mouse whirlin fragments (WiNT, amino acids 1-322; WiCT, amino acids 670-907; GenBank accession, NP_082916.1) were inserted into the expression vector pMALC2X. Recombinant proteins were expressed as N-terminal MBP-fusion proteins in *Escherichia coli* Rosetta cells. The recombinant proteins were purified on amylose resin and were used to immunize rabbits. Whirlin-specific antibodies were affinity-purified from antisera against their respective immunizing antigens immobilized in an agarose bead column (Aminolink; Pierce). Specificity of the antibodies was verified against *Escherichia coli* expressing fusion proteins and against whirlin cDNA clones transiently expressed in a mammalian expression system (HEK293). The polyclonal ORF15 antibody, generated by immunizing a guinea pig with a glutathione *S*-transferase (GST) fusion protein encompassing residues 140-228 of the mouse $RPGR^{ORF15}$ exon, and the rabbit polyclonal S1 antibody, specific for residues 494-563 of all RPGR variants (GenBank accession, NP_001171421.1), have previously been characterized (50,69). Monoclonal rhodopsin antibody, rho-1D4, was a gift from Robert Molday, (University of British Columbia, Vancouver, British Columbia, Canada), and chicken anti-Rootletin antibody was previously published (89). Primary antibodies raised in rabbit were detected with a goat anti-rabbit IgG-horseradish peroxidase conjugate (Pierce) and mouse monoclonal antibodies were detected with a goat anti-mouse IgG-alkaline phosphatase conjugate (Pierce). Alexa fluorochrome-conjugated secondary antibodies for immunostaining were employed (Molecular Probes, Inc).

Immunoblot analyses

For immunoblot analyses, tissues were homogenized in buffer (50mM Tris, pH 7.4, 150mM NaCl, 0.5% NP40) containing a protease inhibitor cocktail (Sigma Aldrich) and were centrifuged at 1000 X g for 2 minutes. Whirlin full-length and short, N-terminal transcripts were subcloned into a pCDNA3.1 vector for mammalian protein expression and were transfected into HEK293 cells as described. For denaturing gel electrophoresis, samples were mixed with 4X SDS sample buffer with β-mercaptoethanol, were separated on 10% polyacrylamide gels and were transferred to PVDF membranes (Immobilon-P, Millipore). After blocking the membrane in 5% skim milk in PBS with 0.1% Tween, immunoreactivities were detected by applying primary antibody overnight followed by the appropriate secondary antibody for 2 hours. As a marker, a Precision Plus Prestained Standard (Biorad), ranging from 10 – 250kD to 25kDa, was used.

Immunohistochemistry

For *in situ* detection of RPGR and whirlin, eyes were embedded in optimal cutting temperature (OCT) compound without fixation and were snap frozen in liquid nitrogen. Cryosections at 10-µm-thick were cut and collected on pretreated glass slides (Superfrost Plus; Fisher Scientific). Sections were stored at -20°C and used within 2 to 3 days. Sections were briefly fixed in 4% paraformaldehyde prior to immunofluorescence staining, which was performed as previously described (50,54).

Dissociated Photoreceptors

Dissociated photoreceptor fragments were obtained by mechanical detachment from freshly dissected mouse retinas, as previously described (72). In brief, retinas were suspended in Ringer Solution and were gently homogenized by five passes through a disposable transfer pipette. Cell fragments were allowed to adhere for 5 minutes to pretreated glass slides (Superfrost Plus Microscope Slides; Fisher Scientific). Adhered cell fragments were fixed for 5 minutes in ice-cold methanol, before proceeding with typical immunocytochemical staining as previously described (50,54).

Results

Identification of RPGR-whirlin interaction using the yeast-two hybrid system

Since $RPGR^{ORF15}$ is preferentially expressed in photoreceptors and appears to be the functionally significant RPGR variant (60), we hypothesized that identifying proteins interacting with the C-terminal domain would provide clues to the physiological significance of these isoforms. We screened a C57BL/6 mouse retinal cDNA library by the yeast two-hybrid system, using the C-terminus of mouse $RPGR^{ORF15}$ ($mRPGR^{ORF15}$) (amino acids 1241-1343) as bait (**Fig. 3.1B**). Of the 92 $HIS3^-$, $ADE2^-$ and lacZ-positive clones that were isolated and sequenced, 20 identical, independent clones coded for the N-terminal region of whirlin, suggesting that $RPGR^{ORF15}$ interacts physically with whirlin. We confirmed that the isolated library plasmid alone did not activate transcription of the reporter genes in yeast when transfected with a control bait protein.

Isolation of an N-terminal whirlin transcript by sequencing analysis of retinal cDNA

Sequence analysis of the whirlin clone isolated from our yeast two-hybrid screen identified an N-terminal whirlin transcript. The highly conserved *whirlin* gene, which comprises 13 exons, is already known to have multiple long and C-terminal short isoforms (see **Table 1**). The long isoforms, which all have an estimated molecular weight of around 100kD, contain three PDZ domains (PDZ_1, PDZ_2 and PDZ_3) and a proline-rich region. There have been four variations of the long isoform reported (GenBank accession, NP_082916.1; NP_001008791.1; NP_001008792.1; NP_001008793.1). The previously reported short C-terminal isoforms (GenBank accession, NP_001008794.1; NP_001008795.1; NP_001008796.1; NP_001008797.4; NP_001008798.1) are the result of variable splicing and multiple start codons in exons 6, 7 and 8. They contain only the PDZ_3 domain and a proline-rich region (87,90) (**Fig. 3.1C**).

The N-terminal transcript identified by our yeast two-hybrid screen, which was recently detected at the transcript but not protein level (91), contains exons one through three followed by inclusion of the third intron and is the first known short N-terminal whirlin transcript. Translation of this variant is expected to result in abrupt truncation of the protein at the beginning of intron three, resulting in a novel, short N-terminal whirlin isoform, subsequently referred to as whirlinNT1 (GenBank accession, HQ148552).
To confirm the existence of this transcript *in vivo*, we reverse transcribed total RNA from C57BL/6 wild type retina, and subsequently amplified the resultant cDNA using

gene specific primers (**Fig. 3.1C**). We were able to successfully amplify and clone this novel whirlin transcript from retinal cDNA. In addition, we also performed 3' RACE on C57BL/6 wildtype retinal cDNA to confirm the existence of a mature mRNA transcript (**Fig. 3.1D**).

Identification of other novel, N-terminal whirlin transcripts

After identifying the novel whirlin transcript from our yeast two-hybrid screen, which is expected to generate a short, N-terminal whirlin isoform, we considered the possibility of other N-terminal variants. Thus, we performed 3' RACE on C57BL/6 wild type retinal cDNA (**Fig. 3.1D**). In addition to confirming the existence of the whirlinNT1 transcript, we identified a second N-terminal whirlin transcript, designated whirlinNT2 (GenBank accession, HQ148553). The whirlinNT2 transcript includes exons 1 through 6 followed by inclusion of intron 7, which results in truncation of the resultant peptide prior to the proline-rich domain (**Fig. 3.1C**). The existence of this transcript was subsequently confirmed by PCR amplification of retinal cDNA (**Fig. 3.1C-D**).

Confirmation of whirlin isoform expression at the protein level in the mouse retina

The tissue specific expression of whirlin was examined by immunoblot analysis. To confirm the existence of the whirlinNT1 and whirlinNT2 transcripts at the protein level, we raised a polyclonal antibody, designated anti-WiNT, designed to recognize the long whirlin isoform as well as any potential N-terminal short whirlin isoforms (**Fig. 3.2A**). In retinal extracts, this antibody detected the 110kDa, full-length whirlin isoform

(GenBank accession, NP_082916.1) previously reported (91) (**Fig. 3.2B**). In addition, we detected two smaller variants around 85kDa and 60kDa and a fourth variant of approximately 34kDa (**Fig. 3.2B**). To confirm that these variants were isoforms of whirlin, the whirlinNT1 and whirlinNT2 transcripts were cloned into a pcDNA3.1 vector and expressed in HEK293 cells (**Fig. 3.2B**). The anti-WiNT polyclonal antibody recognized the whirlinNT1 and whirlinNT2 isoforms from these cell lysates (**Fig. 3.2B**) and the recombinant proteins matched the isoforms observed in retinal extracts. These results confirm the existence of the two novel whirlin transcripts at the protein level and provide an extensive characterization of the N-terminal whirlin splice variants expressed in the mouse retina. Despite extensive efforts, we were unable to identify a whirlin transcript corresponding to the 85kDa band. Although we do not consistently detect this band in retinal extracts, it may be a degradation product, a different N-terminal isoform that we have not identified, non-specific antibody binding or an oligomer. Given that whirlin has been reported to form homodimers (92), the latter is a probable explanation.

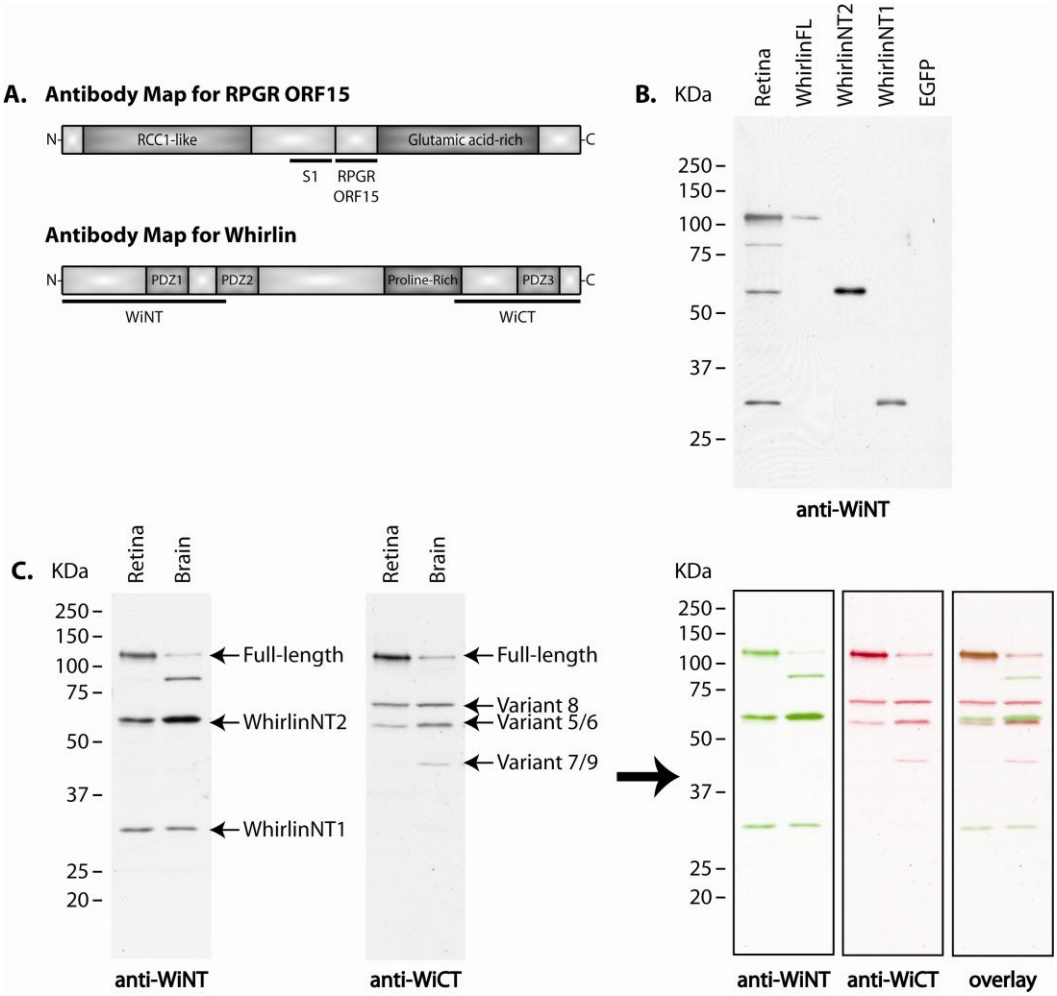

Figure 3.2. Antibody maps for RPGR and whirlin, and analysis of whirlin expression in the mouse retina. (A) *Top:* Illustration of the RPGR^{ORF15} isoform structure and the location of domains used to generate polyclonal antibodies. S1 antibody detects all RPGR isoforms; ORF15 detects only RPGR^{ORF15}. *Bottom:* Schematic representation of the whirlin long isoform structure and location of the domains used to generate polyclonal antibodies against the N-terminal and C-terminal ends. WiNT detects the long whirlin isoform and any potential short, N-terminal isoforms; WiCT also detects the long whirlin isoform as well as the previously reported short, C-terminal isoforms. (B-C) Characterization of whirlin antibodies and analysis of whirlin expression in the mouse retina and brain. (B) Immunoblot analysis of retinal homogenate and cell lysate from HEK293 cells transfected with the designated whirlin isoform. (C) Immunoblot analysis of retinal and cerebral homogenate from C57BL/6 wild type mice. The WiNT antibody detects three major bands of approximately 110kD, 60kD and 34kD in both the retina and brain. We also detect an additional ~85kD band in the brain, which is not consistently detected in the retina and has not been identified. The WiCT antibody detects three major bands of approximately 110kD, 70kD and 60kD in both the retina and brain with an additional ~40kD band only detected in the brain. See **Table 1** for GenBank accession numbers and a description of each known whirlin variant. Artificial colorization and merging of the images confirms that only the 110kD, long whirlin isoform is detectable by both antibodies and that all short N-terminal and C-terminal isoforms are only detected by their respective antibodies.

To look for additional C-terminal isoforms, a polyclonal antibody was raised against the C-terminus of the long whirlin isoform (amino acids 670-907, GenBank accession, NP_082916.1), subsequently referred to as anti-WiCT. The domain used to generate this antibody is illustrated in the antibody map in **Fig. 3.2A**. The calculated molecular weight of the long whirlin isoform is approximately 98kDa however this isoform actually migrates at about 110kDa. We therefore conclude that the additional isoforms recognized by the anti-WiCT antibody (Fig. 2C) correspond to the previously reported C-terminal short isoforms with calculated molecular weights ranging between 38.5kDa and 58.7kDa.

To further validate that both whirlin antibodies recognized the long whirlin isoform, the WiCT antibody was labeled with a horseradish peroxidase tag to eliminate the necessity for a secondary antibody in detection. This permitted sequential probing of the same blot with our anti-WiNT and anti-WiCT antibodies without any background signal during detection of the second antibody. Using Adobe Photoshop, we assigned colors to and superimposed these images to emphasize that both anti-WiNT and anti-WiCT antibodies detect the long whirlin isoform, and that each antibody detects a unique set of alternative, short whirlin isoforms (**Fig 3.2C**).

$RPGR^{ORF15}$ directly interacts with the novel USH2D protein isoform, whirlinNT1

Having verified the presence of multiple whirlin polypeptides in the retina, the $RPGR^{ORF15}$ – whirlin interaction was first validated by MBP pull-down assays, in which

a single 75 kDa mRPGR^{ORF15} isoform was incubated with recombinant MBP-whirlinNT1 fusion protein or MBP alone. Increasing molar concentrations (0.625mM, 1.875mM and 5.625mM) of MBP-whirlinNT1 incrementally increased the amount of bound RPGR^{ORF15} (**Fig. 3.3A**). Interaction between mRPGR^{ORF15} and the equivalent molar concentrations of MBP alone could not be detected.

Recombinant domains of whirlin were then used to identify the RPGR^{ORF15} binding domain through another series of MBP pull-down assays. Four MBP-tagged constructs were tested: (i) a construct containing a full PDZ_1 domain and truncated PDZ_2 domain; (ii) the PDZ_1 domain only; (iii) the PDZ_2 domain only; and (iv) MBP fused to the linker region between the two PDZ domains **(Fig. 3.3B)**. The whirlin PDZ_1 and PDZ_2 domains were identified as independent binding sites for the C-terminus of RPGR^{ORF15} (**Fig. 3.3B**). Importantly, mRPGR^{ORF15} exhibited the highest affinity for whirlin construct containing both PDZ domains, suggesting these two domains act cooperatively in whirlin binding. Interaction of neither the MBP-tagged linker domain nor MBP alone could be detected. Thus, we concluded that whirlin and RPGR are interacting proteins and that whirlin binds via both PDZ_1 and PDZ_2 domains to the C-terminal end of RPGR^{ORF15}.

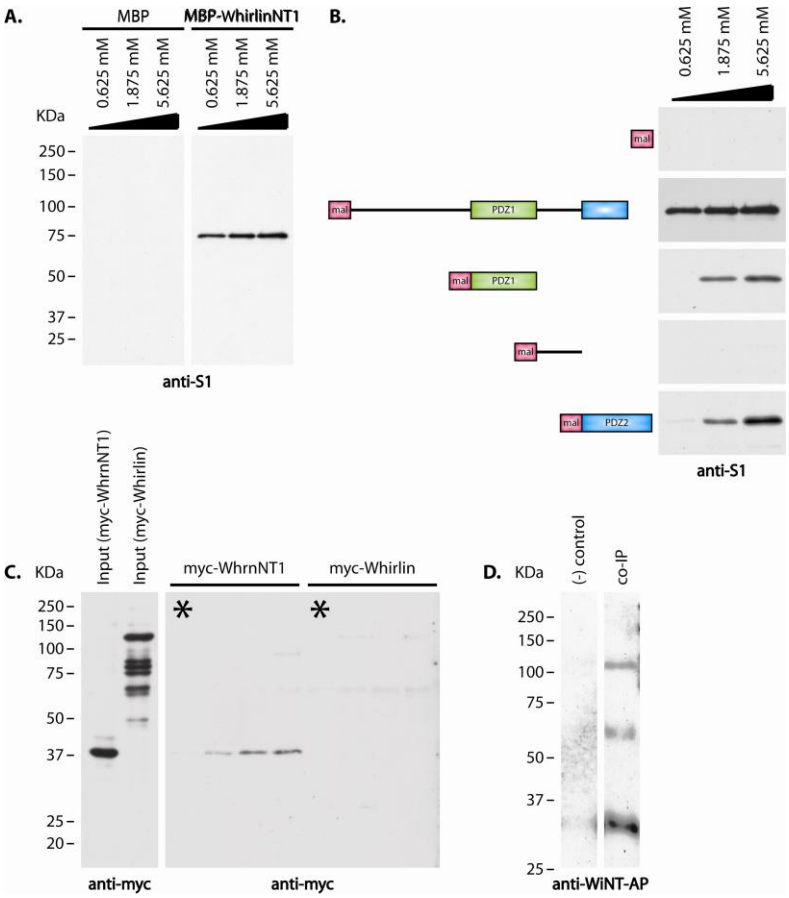

Figure 3.3. Confirmation and analysis of RPGR^{ORF15}/whirlin interaction. (A) Extracts of transfected HEK293 cells expressing a 75kD RPGR^{ORF15} isoform were incubated with immobilized MBP-tagged whirlinNT1 isoform (0.625mM, 1.875mM and 5.625mM) or MBP alone (0.625mM, 1.875mM and 5.625mM). Bound RPGR was analyzed by immunoblot with the S1 antibody to identify RPGR isoforms. (B) Schematic representation of the various whirlin constructs used and immunoblot analysis of pull-down assays used to identify RPGR^{ORF15} binding domain. *From top:* MBP protein (negative control); MBP-whirlinNT1 isoform (positive control); MBP-whirlin PDZ_1 domain; MBP-whirlin inter PDZ_1/PDZ_2 domain; MBP-whirlin PDZ_2 domain. Increasing molar concentrations (0.625mM, 1.875mM and 5.625mM) of each fusion protein were immobilized on amylose resin and were incubated with equal amounts of HEK293 cells lysate expressing a 75kD RPGR^{ORF15} isoform. (C) Comparison of RPGR^{ORF15} interaction with the whirlinNT1 isoform and the long whirlin isoform. *Left*: myc-tagged whirlinNT1 and whirlin long isoforms from transfected HEK293 cells. The smaller bands in the whirlin long isoform lane are degraded protein detected by the myc antibody. *Right*: Immunoblot of binding assay. Increasing amounts of MBP-ORF15 fusion protein were incubated with fixed amounts of either the myc-tagged whirlin NT1 or the myc-tagged long whirlin isoform. The lanes marked by an asterisk indicate the negative control in which MBP was substituted at the highest molar concentration of MBP-ORF15 fusion protein. (D) Immunoblot of co-immunoprecipitation to confirm RPGR^{ORF15}/whirlin interaction *in vivo*. RPGR was immunoprecipitated from RPGRIP knockout retinal homogenate using anti-S1 antibody. Bound protein was analyzed by immunoblot using alkaline phosphatase tagged anti-WiNT antibody. *Left:* Negative control of immunoprecipitation using pre-inoculated antisera in place of anti-S1 antibody. *Right:* Immunoprecipitation using anti-S1 antibody.

Analysis of RPGR^{ORF15} interaction with the full-length whirlin isoform

To further characterize the significance of the RPGR^{ORF15} – whirlin interaction, we sought to identify whether full-length whirlin was also capable of interacting with RPGR^{ORF15}. We incubated the recombinant MBP-tagged RPGR^{ORF15} C-terminal domain (amino acids 1241-1343) with equimolar concentrations of myc-tagged whirlinNT1 or myc-tagged full-length whirlin and immunoprecipitated with anti-myc antibodies **(Fig. 3.3C)**. A recombinant MBP served as a control. As expected, neither whirlin isoform interacted with MBP alone **(Fig. 3.3C, asterisks)**. Although we detected an interaction between myc-whirlinNT1 and MBP-tagged RPGR^{ORF15} C-terminus, we were unable to detect an interaction between the full length myc-whirlin and MBP-tagged RPGR^{ORF15} C-terminus (**Fig. 3.3C**). Two possibilities could explain the failure to detect binding between RPGR^{ORF15} and full-length whirlin. First, the protein conformation of the full-length whirlin isoform may result in structural inhibition of its interaction with RPGR^{ORF15}. Second, whirlin is characterized by the presence of three PDZ domains, which are protein scaffold domains known to form complexes with a number of other proteins. It is our hypothesis that the multitude of potential interactions between the three PDZ domains in full-length whirlin and other proteins in non-neuronal cell lysates may interfere with our binding assay. If this is correct, then it may be possible to detect interactions between RPGR^{ORF15} and full-length whirlin in retinal extracts.

In vivo confirmation of RPGR^{ORF15}/whirlin interaction

To confirm that RPGR^{ORF15} interacts with the WhirlinNT1 isoform *in vivo* and to further examine whether RPGR^{ORF15} interacts with full-length whirlin, RPGR was immunoprecipitated from retinal homogenates using the anti-S1 antibody (50,69). As a negative control, pre-inoculated rabbit serum was used in place of the anti-S1 antibody. Initial attempts to immunoprecipitate RPGR from wild type retinas failed to pull down detectable levels of either whirlin or RPGR (data not shown). In wild type retinas, RPGR forms a high affinity complex with RPGRIP at the connecting cilium and very little soluble RPGR protein is available for immunoprecipitation (50). RPGR was therefore immunoprecipitated from retinal lysates of *Rpgrip*$^{-/-}$ knockout mice (50,51) and the bound whirlin was detected with anti-WiNT antibodies **(Fig. 3.3D)**. RPGR^{ORF15}. Co-immunoprecipitated protein was then analyzed by immunoblot analysis using the polyclonal, N-terminal whirlin antibody, designated anti-WiNT (**Fig. 3.2A**). To eliminate direct interaction of the secondary antibody with the anti-S1/RPGR complex, we tagged our anti-WiNT antibody with an alkaline phosphatase tag such that it could be directly detected by chemiluminescence substrate without subsequent incubation with a secondary antibody. The results from the co-immunoprecipitation assay confirmed our hypothesis that RPGR^{ORF15} specifically interacts with the whirlinNT1 isoform in the mouse retina. In addition, we also confirmed that RPGR^{ORF15} exhibits a physiological interaction with full-length whirlin and the novel whirlinNT2 isoform (**Fig. 3.3D**). These results suggest that the failure to detect an *in vitro* interaction between RPGR^{ORF15} and full-length whirlin is an artifact.

RPGR^{ORF15} colocalizes with whirlin in the mouse retina

RPGR is known to localize in the connecting cilia of both rod and cone photoreceptors (37,50,52,54). Although there have been some conflicting reports regarding localization of whirlin (85,91,93,94), our initial hypothesis and subsequent interpretations are based on previous reports that whirlin does exist in the connecting cilium, as measured by immunogold electron microscopy in both mouse and Xenopus photoreceptors (85), and that whirlin has been shown to precipitate with other proteins found predominantly within the connecting cilium (85,93,94).

Thus, to add further support for a RPGR^{ORF15} – whirlin interaction *in vivo*, subcellular localization of the proteins were analyzed by co-immunostaining. Immunohistochemical analysis of unfixed retinal cryosections detected whirlin in the vicinity of the connecting cilia by both the WiNT and WiCT antibodies. Significantly, whirlin colocalized with RPGR^{ORF15} (**Fig. 3.4A-B**). At the light microscopy level, our results correspond well to numerous publications that show high-magnification images of whirlin co-localizing with markers of the connecting cilium. We were unable, however, to verify previous reports of whirlin in the outer plexiform layer or outer limiting membrane (85).

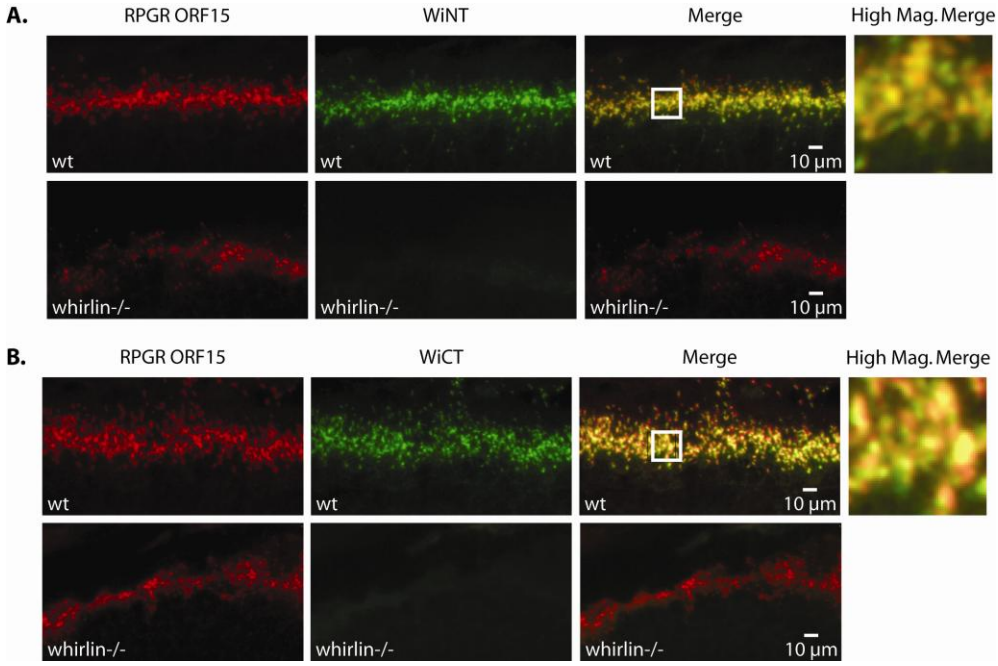

Figure 3.4. Colocalization of whirlin and RPGR^{ORF15} in the mouse retina by immunohistochemical analysis. (A) *Top:* Double staining of C57BL/6 wildtype retina with RPGR ORF15 polyclonal antibody (red) and WiNT polyclonal antibody (green). *Bottom:* Double staining of whirlin knockout retina with RPGR ORF15 polyclonal antibody (red) and WiNT polyclonal antibody (green). (B) *Top:* Double staining of C57BL/6 wildtype retina with RPGR ORF15 polyclonal antibody (red) and WiCT polyclonal antibody (green). *Bottom:* Double staining of whirlin knockout retina with RPGR ORF15 polyclonal antibody (red) and WiCT polyclonal antibody (green). (A-B) The boxed region on the merged images indicates the region shown at right at higher magnification. The higher magnification merged images indicate that both whirlin antibodies partially colocalize with RPGR^{ORF15} in the vicinity of the photoreceptor connecting cilia.

To confirm the specificities of the whirlin antibodies *in vivo*, we also performed immunohistochemistry staining on unfixed retinal cryosections from whirlin knockout mice (**Fig. 3.4A-B**). As expected, whirlin immunoreactivity was not observed in whirlin knockout mice. Also, localization of RPGR^{ORF15} in the connecting cilia is not dependent on whirlin. Our data indicate that whirlin extensively co-localizes with

RPGR^{ORF15} in the photoreceptor connecting cilia and that ciliary localization of RPGR^{ORF15} does not depend on whirlin.

Distribution of whirlin in dissociated photoreceptors

To further examine the co-localization of RPGR^{ORF15} and whirlin at a higher resolution, we performed double labeling for RPGR^{ORF15} and whirlin on dissociated photoreceptors. Immunofluorescence studies on dissociated photoreceptors are commonly done to provide better spatial resolution of certain proteins (54,69,95,96). This approach often provides better staining due to differences in fixation methods and availability of epitopes.

Comparison of the immunofluorescence images double-labeled with our anti-WiNT and anti-RPGR ORF15 antibodies confirmed co-localization of the interacting proteins within the connecting cilium (**Fig. 3.5A; arrowhead**) In addition to localization in the connecting cilia, our WiNT antibody also exhibited punctate staining along the rootlet, as is shown in the co-localization with anti-rootletin antibody in **Fig. 3.5B**. We also co-immunolabeled dissociated photoreceptors using our anti-WiCT and anti-RPGR^{ORF15} antibodies, which again confirmed co-localization of RPGR^{ORF15} and whirlin in the photoreceptor connecting cilia (**Fig. 3.5C**). Our anti-WiCT labeling was not restricted to the connecting cilia and exhibited a punctate staining pattern in the photoreceptor outer segment that colocalized with rhodopsin (**Fig. 3.5D**). We were unable to detect whirlin

localization in the pericilliary region with either antibody due to the physical disruption of the cell used to obtain dissociated photoreceptors fragments.

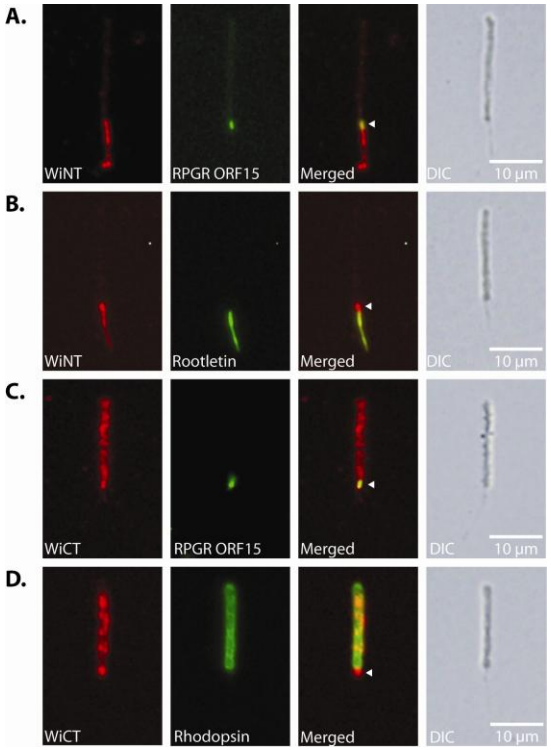

Figure 3.5. Subcellular localization of whirlin isoforms in dissociated retinal photoreceptors. (A) Double staining for whirlin N-terminal isoforms and RPGR^{ORF15}. (B) Double staining for whirlin N-terminal isoforms and Rootletin. (C) Double staining for whirlin C-terminal isoforms and RPGR^{ORF15}. (D) Double staining for whirlin C-terminal isoforms and rhodopsin. Arrowheads indicate areas of colocalization within the connecting cilium.

Thus, immunostaining of dissociated photoreceptors not only confirms the co-localization of RPGR^{ORF15} and whirlin in the connecting cilia, but also demonstrates that the different whirlin isoforms show distinct localization patterns within photoreceptors and therefore may have distinct functions within the subcellular compartments of photoreceptors.

Discussion

Mutations in RPGR are one of the most frequent causes of inherited retinal degeneration. Based on mutational analysis and previous studies of RPGR null and transgenic mice, the photoreceptor specific $RPGR^{ORF15}$ isoforms are essential to photoreceptor maintenance and survival. In this study, we identified the Usher protein whirlin as a novel interactor with RPGR, and by transcriptional and protein analysis of whirlin expression identified two novel N-terminal short whirlin isoforms (**Fig. 6**). Our data also indicate that these short N-terminal variants and the previously reported short C-terminal variants have different subcellular localizations within photoreceptors and thus may retain discrete functions. The whirlin – $RPGR^{ORF15}$ interaction identified in this study provides the first evidence linking $RPGR^{ORF15}$ to the Usher protein network, thereby indirectly connecting $RPGR^{ORF15}$ to a number of other proteins also known to cause RP. The analogous retinal phenotypes associated with mutations in these loci indicate a physiologically significant interaction that may provide further evidence to the function of these proteins in photoreceptors.

WHRN/DFNB31 was first identified as a novel locus responsible for an autosomal recessive form of non-syndromic, congenital deafness, identified as DFNB31 (87). Recently, mutations in whirlin have been found to underlie Usher Syndrome, type IID (USH2D), an autosomal recessive condition that manifests as both congenital hearing loss and visual impairment resulting from retinitis pigmentosa (88). Ebermann et al. (2007) proposed that the genotype-phenotype correlation (non-syndromic deafness vs.

Figure 3.6. Comparison of the long whirlin isoform with the predicted short, N-terminal isoforms expressed in the mouse retina. (**A-B**) The three predicted PDZ domains (amino acid positions 141−216, 280−350 and 815−886) are shown in green, cyan and orange, respectively, and the proline-rich domain (amino acid positions 573−712) is shown in dark blue. (**A**) Schematic representation of the mouse whirlin isoforms showing long, N-terminal and C-terminal short isoforms. Each N-terminal short isoform (WhirlinNT1 and WhirlinNT2) is represented separately to illustrate domain variation, while the C-terminal short isoforms, which are all predicted to encode the same domains, are shown collectively. The zigzag line is shown to indicate variability in the N-terminus of the C-terminal short isoforms. (**B**) Amino acid sequence for the long whirlin isoform and novel N-terminal whirlin isoforms. Predicted stop codons for each isoform are indicated with an asterisk and alternative amino acids are shown in red. The extent of the whirler deletion is marked by a black line.

A. **Whirlin Full-Length Isoform (Wifl)**

WhirlinNT1 Isoform (WiNT1)

WhirlinNT2 Isoform (WiNT2)

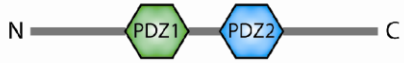

WhirlinCT Isoforms (Variants 5-9)

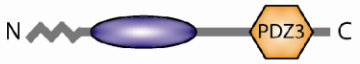

B.

```
Whrn full     MNAQLDGLSV SSSSTGSLGS AAAAAGGGGG AGLRLLSANV RQLHQALTAL LSEPEREQFT
WhrnNT2       MNAQLDGLSV SSSSTGSLGS AAAAAGGGGG AGLRLLSANV RQLHQALTAL LSEPEREQFT
WhrnNT1       MNAQLDGLSV SSSSTGSLGS AAAAAGGGGG AGLRLLSANV RQLHQALTAL LSEPEREQFT

Whrn full     HCLNAYHARR NVFDLVRTLR VLLDSPVKRR LLPMLRLVIP RSDQLLFDQY TAEGLYLPAT
WhrnNT2       HCLNAYHARR NVFDLVRTLR VLLDSPVKRR LLPMLRLVIP RSDQLLFDQY TAEGLYLPAT
WhrnNT1       HCLNAYHARR NVFDLVRTLR VLLDSPVKRR LLPMLRLVIP RSDQLLFDQY TAEGLYLPAT

Whrn full     TPYRQPAWAA PDGAGPGEVR LVSLRRAKAH EGLGFSIRGG SEHGVGIYVS LVEPGSLAEK
WhrnNT2       TPYRQPAWAA PDGAGPGEVR LVSLRRAKAH EGLGFSIRGG SEHGVGIYVS LVEPGSLAEK
WhrnNT1       TPYRQPAWAA PDGAGPGEVR LVSLRRAKAH EGLGFSIRGG SEHGVGIYVS LVEPGSLAEK

Whrn full     EGLRVGDQIL RVNDKSLARV THAEAVKALK GSKKLVLSVY SAGRIPGGYV TNHIYTWVDP
WhrnNT2       EGLRVGDQIL RVNDKSLARV THAEAVKALK GSKKLVLSVY SAGRIPGGYV TNHIYTWVDP
WhrnNT1       EGLRVGDQIL RVNDKSLARV THAEAVKALK GSKKLVLSVY SAGRIPGGYV TNHIYTWVDP

Whrn full     QGRSTSPPSS LPQPHGSTLR QREDDRRSTL HLLQSGDEKK VNLVLGDGRS LGLTIRGGAE
WhrnNT2       QGRSTSPPSS LPQPHGSTLR QREDDRRSTL HLLQSGDEKK VNLVLGDGRS LGLTIRGGAE
WhrnNT1       QGRSTSPPSS LPQPHGSTLR QREDDRRSTL HLLQSGDEKK VNLVLGDGRS LGLTIRGGAE

Whrn full     YGLGIYITGV DPGSEAESSG LKVGDQILEV NGRSFLNILH DEAVKLLKSS RHLILTVKDV
WhrnNT2       YGLGIYITGV DPGSEAESSG LKVGDQILEV NGRSFLNILH DEAVKLLKSS RHLILTVKDV
WhrnNT1       YGLGIYITGV DPGSEAESSG LK*

Whrn full     GRLPHARTTV DQTKWIASSR IGESVANSAG FPGDHTEEGT SKPGFYKGPA GSQVTLSSLG
WhrnNT2       GRLPHARTTV DQTKWIASSR IGESVANSAG FPGDHTEEGT SKPGFYKGPA GSQVTLSSLG

Whrn full     NQTRALLDDQ ARHLLTEQER ATMMYYLAQY RGGTISVEAM VMALFELLNT HAKFSLLSEV
WhrnNT2       NQTRALLDDQ ARHLLTEQER ATMMYYLAQY RGGTISVEAM VMALFELLNT HAKFSLLSEV

Whrn full     RSIISPQDLD RFDHLVLRRE IESMKARQPP GPGVGDTYSM VSYSDTGSST GSHGTSTTVS
WhrnNT2       RSIISPQDLD RFDHLVLRRE IESMKARQPP GPGVGDTYSM VSYSDTGSST GSHGTSTTVS

Whrn full     SARNTLDLEG TGETTQGSTN ALPDVSVDDV KSPSEDLPGI KPPPPPPPLA QGHDRLLGQP
WhrnNT2       SARVSHPCPI LGEKVRARIR CFPPKPRVPH L*

Whrn full     RKPGREDPAP LSSAAHSGIV FSAPRNRSPP PGTAPTPGPS SAQDSPSSPI YASISHANPS

Whrn full     SRKPLDTHLA LVNQHPIGPF PRVQSPPHLK SPPAETPGAG ACLPPPSPSE HPDAVGANQH

Whrn full     FVLVEVHRPD SEPDVNEVRA LPQTRTASTL SQLSDSGQTL SEDSGVDAGE TEASTSGRGR

Whrn full     QTASAKNKNG KEQPRTERTA EGANKPPGLL EPTSTLVRVR KSAATLGIAI EGGANTRQPL

Whrn full     PRIVTIQRGG SAHNCGQLKV GHVILEVNGQ TLRGKEHKEA AQIIAEAFKT KERDYIDFLV

Whrn full     TEFNVML*
```

USH2D) may be dependent on the location of a given mutation within the whirlin gene locus. While the first disease-causing mutations identified in humans truncated the protein close to its C-terminus and caused DFNB31, they reported compound heterozygosity affecting the integrity of the 5' end of the *WHRN* gene as the causative loci in a patient with USH2D. Their theory was further supported in a recent study (91) comparing a whirlin knockout mouse to the whirler mouse. The *whirler* mouse has a large deletion in the 3' end of the whirlin gene (**Fig. 3.6B**) and is phenotypically similar to DFNB31 patients (90); however, targeted deletion of the whirlin gene, which affects both the long and short, C-terminal whirlin variants, results in both retinal and inner ear defects that resemble the human USH2D phenotype (91). Our study, however, provides the first physiological evidence to suggest such phenotypic differences reflect the variable protein interactions, subcellular localization, and likely independent function of the short N-terminal and C-terminal whirlin isoforms.

First and foremost, our key finding is the identification of a novel interaction between whirlin and $RPGR^{ORF15}$. Since $RPGR^{ORF15}$ interacts with the PDZ_1 and PDZ_2 domains of whirlin, our data imply that these N-terminal domains retain an important functional role in photoreceptors. Furthermore, identification of two short, N-terminal whirlin isoforms suggests that not only do the N-terminal PDZ domains boast specific and distinct interactions, but that differential expression of the whirlin gene produces both N-terminal and C-terminal variants. In contrast to the previously reported C-terminal variants, which encode the PDZ_3 domain and proline-rich region, the first of these novel

N-terminal isoforms encodes only the PDZ_1 domain and undergoes internal truncation within the PDZ_2 domain, while the second encodes both the PDZ_1 and PDZ_2 domains (**Fig. 6**). This indicates that whirlin undergoes alternative splicing to produce variable isoforms, each possessing a unique combination of domains and potentially independent function.

In summary, the data in this study clearly demonstrate that direct protein-protein interaction between $RPGR^{ORF15}$ and whirlin connects $RPGR^{ORF15}$ to the extensive Usher protein network. This study also shows the presence of two novel, N-terminal short whirlin variants at the mRNA and protein level and further validates the significance of the integrity of the 5' end of the *whirlin/DFNB31* gene in photoreceptor function and survival. Future investigations into the relationship of $RPGR^{ORF15}$ and the Usher protein network may provide further insight into the function of the ORF15 isoforms as well as the physiology of this growing 'interactome'.

Mutations in *RPGR* are one of the most frequent causes of inherited retinal degeneration. Based on mutational analysis and previous studies of RPGR null and transgenic mice, the photoreceptor specific $RPGR^{ORF15}$ isoforms are essential to photoreceptor maintenance and survival. In this study, we identified the Usher protein whirlin as a novel interactor with RPGR, and by transcriptional and protein analysis of whirlin expression identified two novel N-terminal short whirlin isoforms (**Fig. 6**). Our data also indicate that these short N-terminal variants and the previously reported short C-

terminal variants have different subcellular localizations within photoreceptors and thus may retain discrete functions. The whirlin – $RPGR^{ORF15}$ interaction identified in this study provides the first evidence linking $RPGR^{ORF15}$ to the Usher protein network, thereby indirectly connecting $RPGR^{ORF15}$ to a number of other proteins also known to cause RP. The analogous retinal phenotypes associated with mutations in these loci indicate a physiologically significant interaction that may provide further evidence to the function of these proteins in photoreceptors.

CHAPTER IV

CONCLUSIONS

Summary

An important finding of this work is that *Rpgr* expression exhibits dynamic temporal regulation during retinal development and that Rpgr variants exhibit variability toward localization in the connecting cilia of mature photoreceptors. Previous analyses of Rpgr-null mice report that mammalian photoreceptors undergo normal physiological development despite an absence of Rpgr (54), suggesting that Rpgr is not required for development. However, the temporal regulation of Rpgr taken together with the robust expression of the $Rpgr^{ex1-19}$ variant during retinal development is nonetheless suggestive of a functional role for Rpgr in cellular development. In addition, we report that emergence of the $Rpgr^{ORF15}$ variants follows a reciprocal expression pattern, coinciding with photoreceptor maturation. This finding upholds the long held notion that $Rpgr^{ORF15}$ plays an essential role in sustaining the normal physiology of mature photoreceptors (54). While it has been speculated that $Rpgr^{ORF15}$ is the only functionally significant variant in photoreceptors (60), the dynamics of Rpgr expression in emerging photoreceptors described herein suggests that both the $Rpgr^{ORF15}$ and $Rpgr^{ex1-19}$ variants retain some independent, isoform specific functions.

In this study, we also use transgenic mouse models to examine the phenotypic effects of gross overexpression of the $Rpgr^{ex1-19}$ and $Rpgr^{ORF15}$ variants in photoreceptors and to

evaluate whether the Rpgr^{ex1-19} variant alone is capable of restoring function to photoreceptors lacking endogenous Rpgr. Although transgenic expression of both variants exhibits normal ciliary localization, misexpression of the Rpgr^{ex1-19} variant results in abnormal accumulation of Rpgr in photoreceptor outer segments. Interaction of the Rpgr^{ex1-19} variant with the membranous outer segments results in unusual histopathological changes in outer segment morphology. The severity of the disease course is substantially more acute than that described in previous reports of Rpgr null mutant mice (54). Interestingly, photoreceptors tolerate overexpression of the Rpgr^{ORF15} variant without evidence of degeneration. Since similar misexpression of the Rpgr^{ORF15} variant results in neither atypical accumulation of protein in the outer segment nor a degenerative retinal phenotype, we conclude that our report describes an Rpgr^{ex1-19} specific phenomenon rather than a non-specific consequence associated with the intense level of overexpression.

Given that the Rpgr^{ex1-19} variant differs from the Rpgr^{ORF15} variant by the presence of a C-terminal isoprenylation motif (25,37,46,79), we hypothesize that the mislocalized accumulation of excess Rpgr^{ex1-19} protein observed in photoreceptor outer segments by immunofluorescence is likely related to the membranous nature of the outer segment structure and innate properties of the isoprenylation signal. In general, isoprenylation motifs signal the addition of prenyl groups at carboxy-terminal cysteine residues, which are known to anchor proteins to cell membranes (77,78). By electron microscopy, it is clear that accumulation of Rpgr^{ex1-19} protein in the photoreceptor outer segments both

functionally and morphologically disrupts the organized structure of the outer segments' membranous disks.

With diminished expression of endogenous Rpgr^{ex1-19} in mature photoreceptors and the affinity of Rpgr^{ex1-19} to tightly bind Rpgrip in the connecting cilia(44,45,50), the presence of Rpgrip is likely sufficient to limit localization of endogenous Rpgr to the connecting cilia. This would suggest that if the concentration of Rpgr^{ex1-19} exceeds the binding capacity of Rpgrip or if binding is otherwise interrupted, default may begin to mislocalize and accumulate in the photoreceptor outer segments, as is observed in our transgenic mouse model.

Although endogenous Rpgr^{ex1-19} expression in adult photoreceptors is minimal, further investigation of this artificial system may nonetheless provide evidence of native Rpgr^{ex1-19} function in developing and/or mature photoreceptors, and may reveal the importance of proper down-regulation of the Rpgr^{ex1-19} variant in mature cells. For example, isoprenylation of Rpgr may be required for some form of ciliary trafficking during very early stages of photoreceptor development before the appearance of the outer segments. Thus, the Rpgr^{ex1-19} variants may possess different functions during early development when expression is robust, as compared to the function of Rpgr^{ORF15} following ciliogenesis and outer segment maturation.

The reciprocal emergence of the Rpgr^{ORF15} variant, described herein, which coincides with photoreceptor maturation, further supports the long held hypothesis, based on mutational analysis and previous studies of Rpgr null and transgenic mice, that the photoreceptor specific Rpgr^{ORF15} isoforms are essential to the maintenance and survival of mature photoreceptors (60). Such an independent function would suggest that the domain encoded by exon ORF14/15, which differentiates between the Rpgr^{ex1-19} and Rpgr^{ORF15} variants, should have unique interacting partners in the retina. Thus, we used a yeast two-hybrid screen to further elucidate the function of the ORF15 variants by identifying potential interacting partners of the C-terminus of Rpgr^{ORF15}.

We identified the Usher protein whirlin, a putative PDZ scaffold protein expressed in cochlear hair cells and retinal photoreceptors, as a novel interactor of Rpgr^{ORF15}. Mutations in the *whirlin* (*WHRN/DFNB31*) locus are responsible for DFNB31, an autosomal recessive form of non-syndromic, congenital deafness (87), and Usher Syndrome, type IID (USH2D), an autosomal recessive condition characterized by both congenital hearing loss and visual impairment resulting from retinitis pigmentosa (88). The physiologically significant whirlin-Rpgr^{ORF15} interaction described provides a novel mechanism for the RP phenotype associated with USH2D.

Since whirlin is a member of the extensive Usher protein network, a dynamic complex which includes motor proteins, scaffold proteins, cell adhesion molecules and transmembrane receptors critical for development and maintenance of these

sensorineural cells (80,82-86,97), the direct protein-protein interaction between $Rpgr^{ORF15}$ and whirlin described provides the first evidence connecting Rpgr to the extensive Usher protein network, thereby indirectly connecting $Rpgr^{ORF15}$ to a number of other proteins also known to cause RP. The analogous retinal phenotypes associated with mutations in these loci indicate a physiologically significant interaction that may provide further evidence to the function of these proteins in photoreceptors.

In addition to identifying a direct association between whirlin and $Rpgr^{ORF15}$, we also identified two novel N-terminal short whirlin isoforms by transcriptional and protein analysis of whirlin expression. This indicates that differential expression of the whirlin gene produces N-terminal variants in addition to the previously reported C-terminal variants and that alternative splicing of the whirlin transcript results in expression of variable isoforms possessing a unique combination of domains. Unlike the C-terminal variants, which encode only the proline-rich region and PDZ_3 domain, the first of these novel N-terminal isoforms encodes the PDZ_1 domain and undergoes internal truncation within the PDZ_2 domain, while the second encodes both the PDZ_1 and PDZ_2 domains. Our data also indicate that these short N-terminal variants and C-terminal variants have distinct subcellular localization patterns within photoreceptors.

In conclusion, this study clearly demonstrates that direct protein-protein interaction between $Rpgr^{ORF15}$ and whirlin connects Rpgr to the extensive Usher protein network and also shows the presence of two novel, N-terminal short whirlin variants at the

mRNA and protein level in photoreceptors. Together, these data validate the significance of the integrity of the 5' end of the whirlin/DFNB31 gene in photoreceptor function and survival.

Recommendations

We have previously shown that expression of a single, internally truncated $Rpgr^{ORF15}$ variant substantially rescues the *Rpgr* null phenotype (60). However, since there is a void in knowledge regarding protein expression in RPGR patients, these more recent findings should also be taken into consideration when exploring treatment options using gene therapy. Although a majority of *RPGR* mutations are in the ORF15 exon and only directly affect the $RPGR^{ORF15}$ variants, there is some possibility of indirect effects on $RPGR^{ex1-19}$ expression. Given that all RPGR variants are under the control of a single promoter, it is possible that $RPGR^{ex1-19}$ expression may be affected by endogenous efforts to compensate for the loss of functional $Rpgr^{ORF15}$. If further studies support this theory, then introduction of the $RPGR^{ORF15}$ variant by gene therapy may potentially affect endogenous $RPGR^{ex1-19}$ expression, in which case, up-regulation of $RPGR^{ex1-19}$ expression may prove more detrimental to photoreceptor integrity and incite disease progression than the lack of functional $RPGR^{ORF15}$.

Further investigation of protein expression in RPGR patients would provide valuable information and would be beneficial in alleviating this concern. However, given the difficulty of obtaining retinal tissue samples from RPGR patients prior to disease

progression, well designed studies utilizing cell culture and transgenic mouse models may have to substitute. Since expression of the Rpgr^{ORF15} transgene in the mROIF transgenic line described in this study closely mimics the expression pattern of endogenous Rpgr^{ORF15}, we have generated another mouse model expressing the same construct with a single base-pair deletion in the purine-rich region of the ORF14/15 exon. This mutation is similar to the type of mutations often described in RPGR patients. Transcriptional and protein analysis of this line is expected to provide valuable clues regarding the effects of ORF14/15 mutations on the complex internal splicing of the RPGR^{ORF15} variants. We have also found that transient transfection of HEK293 cells with our wild-type and mutant RpgrORF15 transgenic constructs results in expression patterns similar to that seen in retinal homogenate from the transgenic mice. Utilization of this *in vitro* system would be a more efficient and cost-effective method for examining the affects of various types of mutations. Because of the unpredictability of internal splicing in the ORF14/15 exon, transitions, transversions, insertions and deletions in the purine-rich region may have unexpected impacts on the protein sequence. In addition to producing an Rpgr^{ORF15} specific polyclonal antibody to recognize the C-terminus of the ORF15 domain, we also recommended designing expression constructs with three C-terminal frame-shift tags so that the affects of splicing at the protein level may be assessed by immunoblot utilizing tag-specific antibodies.

Although these experiments would provide valuable insight relating to endogenous $Rpgr^{ORF15}$ expression and the effects of ORF15 mutations on protein expression, these studies would not be sufficient in alleviating the previously mentioned concerns regarding the single Rpgr promoter and the effects of $Rpgr^{ORF15}$ mutations on $Rpgr^{ex1-19}$ expression. Thus, we recommend generating a mutant $Rpgr^{ORF15}$ knock-in mouse model for additional studies. This would provide an excellent model for future gene therapy studies.

REFERENCES

1. Mann, I. (1964) *The development of the human eye*, Grune and Stralton, New York

2. Cajal, S. R.y. (1894) *Die Retina der Wirbelthiere: Untersuchungen mit der Golgi-cajal'schen Chromsilbermethode und der ehrlich'schen Methylenblaufärbung*, translated by R. Greef. Bergman,Wiesbaden

3. Cajal, S. R.y. (1991) *Cajal's Degeneration and Regeneration of the Nervous System*, Oxford University Press, New York

4. Kolb, H., Nelson, R., Ahnelt, P., and Cuenca, N. (2001) *Prog. Brain Res.* **131**, 3-26

5. Kolb, H. (1991) The neural organization of the human retina in *Principles and practices of clinical electrophysiology of vision* (Heckenlively JR, Arden GB. ed.), Mosby Year Book Inc, St. Louis. pp 25-52

6. Rodieck, R. (1973) *The vertebrate retina: principles of structure and function*, W.H. Freeman and Company, San Francisco

7. Polyak, S. (1941) *The retina*, University of Chicago Press, Chicago

8. Mustafi, D., Engel, A. H., and Palczewski, K. (2009) *Prog. Retin. Eye Res.* **28**, 289-302

9. Linberg, K., Cuenca, N., Ahnelt, P., Fisher, S., and Kolb, H. (2001) *Prog. Brain Res.* **131**, 27-52

10. Steinberg, R. H., Fisher, S. K., and Anderson, D. H. (1980) *J. Comp. Neurol.* **190**, 501-508

11. Young, R. W. (1971) *J. Cell Biol.* **49**, 303-318

12. Nathans, J. (1992) *Biochemistry* **31**, 4923-4931

13. Nathans, J. (1990) *Cold Spring Harb. Symp. Quant. Biol.* **55**, 621-633

14. Nathans, J., Thomas, D., and Hogness, D. S. (1986) *Science* **232**, 193-202

15. Hargrave, P. A., and McDowell, J. H. (1992) *Int. Rev. Cytol.* **137B**, 49-97

16. Hosch, J., Lorenz, B., and Stieger, K. (2011) *Ophthalmic. Genet.* **32**, 1-11

17. Haim, M. (2002) *Acta. Ophthalmol. Scand. Suppl.*, 1-34

18. Kennan, A., Aherne, A., and Humphries, P. (2005) *Trends Genet.* **21**, 103-110

19. Hartong, D. T., Berson, E. L., and Dryja, T. P. (2006) *Lancet* **368**, 1795-1809

20. Bunker, C. H., Berson, E. L., Bromley, W. C., Hayes, R. P., and Roderick, T. H. (1984) *Am. J. Ophthalmol.* **97**, 357-365

21. Fishman, G. A. (1978) *Arch. Ophthalmol.* **96**, 822-826

22. Boughman, J. A., Conneally, P. M., and Nance, W. E. (1980) *Am. J. Hum. Genet.* **32**, 223-235

23. Jay, M. (1982) *Br. J. Ophthalmol.* **66**, 405-416

24. Goldberg, A. F., and Molday, R. S. (1996) *Proc. Natl. Acad. Sci. U S A* **93**, 13726-13730

25. Meindl, A., Dry, K., Herrmann, K., Manson, F., Ciccodicola, A., Edgar, A., Carvalho, M. R., Achatz, H., Hellebrand, H., Lennon, A., Migliaccio, C., Porter, K., Zrenner, E., Bird, A., Jay, M., Lorenz, B., Wittwer, B., D'Urso, M., Meitinger, T., and Wright, A. (1996) *Nat. Genet.* **13**, 35-42

26. Vervoort, R., Lennon, A., Bird, A. C., Tulloch, B., Axton, R., Miano, M. G., Meindl, A., Meitinger, T., Ciccodicola, A., and Wright, A. F. (2000) *Nat. Genet.* **25**, 462-466

27. Ferreira, P. A. (2005) *Human Molecular Genetics* **14**, R259-R267

28. Breuer, D. K., Yashar, B. M., Filippova, E., Hiriyanna, S., Lyons, R. H., Mears, A. J., Asaye, B., Acar, C., Vervoort, R., Wright, A. F., Musarella, M. A., Wheeler, P., MacDonald, I., Iannaccone, A., Birch, D., Hoffman, D. R., Fishman, G. A., Heckenlively, J. R., Jacobson, S. G., Sieving, P. A., and Swaroop, A. (2002) *Am. J. Hum. Genet.* **70**, 1545-1554

29. Roepman, R., Bauer, D., Rosenberg, T., van Duijnhoven, G., van de Vosse, E., Platzer, M., Rosenthal, A., Ropers, H. H., Cremers, F. P., and Berger, W. (1996) *Hum. Mol. Genet.* **5**, 827-833

30. Sharon, D., Sandberg, M. A., Rabe, V. W., Stillberger, M., Dryja, T. P., and Berson, E. L. (2003) *Am. J. Hum. Genet.* **73**, 1131-1146

31. Demirci, F. Y., Rigatti, B. W., Wen, G., Radak, A. L., Mah, T. S., Baic, C. L., Traboulsi, E. I., Alitalo, T., Ramser, J., and Gorin, M. B. (2002) *Am. J. Hum. Genet.* **70**, 1049-1053

32. Yang, Z., Peachey, N. S., Moshfeghi, D. M., Thirumalaichary, S., Chorich, L., Shugart, Y. Y., Fan, K., and Zhang, K. (2002) *Hum. Mol. Genet.* **11**, 605-611

33. Ayyagari, R., Demirci, F. Y., Liu, J., Bingham, E. L., Stringham, H., Kakuk, L. E., Boehnke, M., Gorin, M. B., Richards, J. E., and Sieving, P. A. (2002) *Genomics* **80**, 166-171

34. Dasso, M. (1993) *Trends Biochem. Sci.* **18**, 96-101

35. Ohtsubo, M., Kai, R., Furuno, N., Sekiguchi, T., Sekiguchi, M., Hayashida, H., Kuma, K., Miyata, T., Fukushige, S., Murotsu, T., and et al. (1987) *Genes Dev.* **1**, 585-593

36. Gorlich, D., and Mattaj, I. W. (1996) *Science* **271**, 1513-1518

37. Yan, D., Swain, P. K., Breuer, D., Tucker, R. M., Wu, W., Fujita, R., Rehemtulla, A., Burke, D., and Swaroop, A. (1998) *J. Biol. Chem.* **273**, 19656-19663

38. Zito, I., Thiselton, D. L., Gorin, M. B., Stout, J. T., Plant, C., Bird, A. C., Bhattacharya, S. S., and Hardcastle, A. J. (1999) *Hum. Genet.* **105**, 57-62

39. Zito, I., Downes, S. M., Patel, R. J., Cheetham, M. E., Ebenezer, N. D., Jenkins, S. A., Bhattacharya, S. S., Webster, A. R., Holder, G. E., Bird, A. C., Bamiou, D. E., and Hardcastle, A. J. (2003) *J. Med. Genet.* **40**, 609-615

40. Iannaccone, A., Breuer, D. K., Wang, X. F., Kuo, S. F., Normando, E. M., Filippova, E., Baldi, A., Hiriyanna, S., MacDonald, C. B., Baldi, F., Cosgrove, D., Morton, C. C., Swaroop, A., and Jablonski, M. M. (2003) *J. Med. Genet.* **40**, e118

41. Dry, K. L., Manson, F. D., Lennon, A., Bergen, A. A., Van Dorp, D. B., and Wright, A. F. (1999) *Hum. Mutat.* **13**, 141-145

42. van Dorp, D. B., Wright, A. F., Carothers, A. D., and Bleeker-Wagemakers, E. M. (1992) *Hum. Genet.* **88**, 331-334

43. Linari, M., Ueffing, M., Manson, F., Wright, A., Meitinger, T., and Becker, J. (1999) *Proc. Natl. Acad. Sci. U S A* **96**, 1315-1320

44. Boylan, J. P., and Wright, A. F. (2000) *Hum. Mol. Genet.* **9**, 2085-2093

45. Roepman, R., Bernoud-Hubac, N., Schick, D. E., Maugeri, A., Berger, W., Ropers, H. H., Cremers, F. P., and Ferreira, P. A. (2000) *Hum. Mol. Genet.* **9**, 2095-2105

46. Shu, X., Black, G. C., Rice, J. M., Hart-Holden, N., Jones, A., O'Grady, A., Ramsden, S., and Wright, A. F. (2007) *Hum. Mutat.* **28**, 322-328

47. Zito, I., Morris, A., Tyson, P., Winship, I., Sharp, D., Gilbert, D., Thiselton, D. L., Bhattacharya, S. S., and Hardcastle, A. J. (2000) *Hum. Mutat.* **16**, 273-274

48. Li, Y., Dong, B., Hu, A. L., Cui, T. T., and Zheng, Y. Y. (2005) *Zhonghua Yi Xue Yi Chuan Xue Za Zhi* **22**, 396-398

49. Rozet, J. M., Perrault, I., Gigarel, N., Souied, E., Ghazi, I., Gerber, S., Dufier, J. L., Munnich, A., and Kaplan, J. (2002) *J. Med. Genet.* **39**, 284-285

50. Hong, D. H., Yue, G., Adamian, M., and Li, T. (2001) *J. Biol. Chem.* **276**, 12091-12099

51. Zhao, Y., Hong, D. H., Pawlyk, B., Yue, G., Adamian, M., Grynberg, M., Godzik, A., and Li, T. (2003) *Proc. Natl. Acad. Sci. U S A* **100**, 3965-3970

52. Khanna, H., Hurd, T. W., Lillo, C., Shu, X., Parapuram, S. K., He, S., Akimoto, M., Wright, A. F., Margolis, B., Williams, D. S., and Swaroop, A. (2005) *J. Biol. Chem.* **280**, 33580-33587

53. Shu, X., Fry, A. M., Tulloch, B., Manson, F. D., Crabb, J. W., Khanna, H., Faragher, A. J., Lennon, A., He, S., Trojan, P., Giessl, A., Wolfrum, U., Vervoort, R., Swaroop, A., and Wright, A. F. (2005) *Hum. Mol. Genet.* **14**, 1183-1197

54. Hong, D. H., Pawlyk, B. S., Shang, J., Sandberg, M. A., Berson, E. L., and Li, T. (2000) *Proc. Natl. Acad. Sci. U S A* **97**, 3649-3654

55. Sandberg, M. A., Rosner, B., Weigel-DiFranco, C., Dryja, T. P., and Berson, E. L. (2007) *Invest. Ophthalmol. Vis. Sci.* **48**, 1298-1304

56. Grover, S., Fishman, G. A., Anderson, R. J., and Lindeman, M. (2000) *Ophthalmology* **107**, 386-396

57. Souied, E., Segues, B., Ghazi, I., Rozet, J. M., Chatelin, S., Gerber, S., Perrault, I., Michel-Awad, A., Briard, M. L., Plessis, G., Dufier, J. L., Munnich, A., and Kaplan, J. (1997) *J. Med. Genet.* **34**, 793-797

58. Banin, E., Mizrahi-Meissonnier, L., Neis, R., Silverstein, S., Magyar, I., Abeliovich, D., Roepman, R., Berger, W., Rosenberg, T., and Sharon, D. (2007) *Am. J. Med. Genet.* **143A**, 1150-1158

59. Hong, D. H., Pawlyk, B. S., Adamian, M., and Li, T. (2004) *Invest. Ophthalmol. Vis. Sci.* **45**, 36-41

60. Hong, D. H., Pawlyk, B. S., Adamian, M., Sandberg, M. A., and Li, T. (2005) *Invest. Ophthalmol. Vis. Sci.* **46**, 435-441

61. Dryja, T. P., Adams, S. M., Grimsby, J. L., McGee, T. L., Hong, D. H., Li, T., Andreasson, S., and Berson, E. L. (2001) *Am. J. Hum. Genet.* **68**, 1295-1298

62. Gerber, S., Perrault, I., Hanein, S., Barbet, F., Ducroq, D., Ghazi, I., Martin-Coignard, D., Leowski, C., Homfray, T., Dufier, J. L., Munnich, A., Kaplan, J., and Rozet, J. M. (2001) *Eur. J. Hum. Genet.* **9**, 561-571

63. Koenekoop, R. K. (2005) *Ophthalmic. Genet.* **26**, 175-179

64. Zhang, Q., Acland, G. M., Wu, W. X., Johnson, J. L., Pearce-Kelling, S., Tulloch, B., Vervoort, R., Wright, A. F., and Aguirre, G. D. (2002) *Hum. Mol. Genet.* **11**, 993-1003

65. Shu, X., Zeng, Z., Gautier, P., Lennon, A., Gakovic, M., Patton, E. E., and Wright, A. F. (2010) *Hum. Mol. Genet.* **19**, 657-670

66. Berson, E. L., Gouras, P., Gunkel, R. D., and Myrianthopoulos, N. C. (1969) *Arch. Ophthalmol.* **81**, 215-225

67. Kirschner, R., Rosenberg, T., Schultz-Heienbrok, R., Lenzner, S., Feil, S., Roepman, R., Cremers, F. P., Ropers, H. H., and Berger, W. (1999) *Hum. Mol. Genet.* **8**, 1571-1578

68. Hong, D. H., and Li, T. (2002) *Invest. Ophthalmol. Vis. Sci.* **43**, 3373-3382

69. Hong, D. H., Pawlyk, B., Sokolov, M., Strissel, K. J., Yang, J., Tulloch, B., Wright, A. F., Arshavsky, V. Y., and Li, T. (2003) *Invest. Ophthalmol. Vis. Sci.* **44**, 2413-2421

70. Chiu, M. I., and Nathans, J. (1994) *Vis. Neurosci.* **11**, 773-780

71. Li, T., Sandberg, M. A., Pawlyk, B. S., Rosner, B., Hayes, K. C., Dryja, T. P., and Berson, E. L. (1998) *Proc. Natl. Acad. Sci. U S A* **95**, 11933-11938

72. Muresan, V., Joshi, H. C., and Besharse, J. C. (1993) *J. Cell Sci.* **104 (Pt 4)**, 1229-1237

73. Connolly, S. E., Hores, T. A., Smith, L. E., and D'Amore, P. A. (1988) *Microvasc. Res.* **36**, 275-290

74. Livesey, F. J., and Cepko, C. L. (2001) *Nat. Rev. Neurosci.* **2**, 109-118

75. Dorrell, M. I., Aguilar, E., Weber, C., and Friedlander, M. (2004) *Invest. Ophthalmol. Vis. Sci.* **45**, 1009-1019

76. McGee Sanftner, L. H., Abel, H., Hauswirth, W. W., and Flannery, J. G. (2001) *Mol. Ther.* **4**, 622-629

77. Zhang, F. L., and Casey, P. J. (1996) *Annu. Rev. Biochem.* **65**, 241-269

78. Clarke, S. (1992) *Annu. Rev. Biochem.* **61**, 355-386

79. Wright, A. F., and Shu, X. (2007) *Exp. Eye Res.* **85**, 1-2

80. Reiners, J., van Wijk, E., Marker, T., Zimmermann, U., Jurgens, K., te Brinke, H., Overlack, N., Roepman, R., Knipper, M., Kremer, H., and Wolfrum, U. (2005) *Hum. Mol. Genet.* **14**, 3933-3943

81. Reiners, J., Nagel-Wolfrum, K., Jurgens, K., Marker, T., and Wolfrum, U. (2006) *Exp. Eye Res.* **83**, 97-119

82. Kremer, H., van Wijk, E., Marker, T., Wolfrum, U., and Roepman, R. (2006) *Hum. Mol. Genet.* **15 Spec No 2**, R262-270

83. El-Amraoui, A., and Petit, C. (2005) *J. Cell Sci.* **118**, 4593-4603

84. Adato, A., Michel, V., Kikkawa, Y., Reiners, J., Alagramam, K. N., Weil, D., Yonekawa, H., Wolfrum, U., El-Amraoui, A., and Petit, C. (2005) *Hum. Mol. Genet.* **14**, 347-356

85. Maerker, T., van Wijk, E., Overlack, N., Kersten, F. F., McGee, J., Goldmann, T., Sehn, E., Roepman, R., Walsh, E. J., Kremer, H., and Wolfrum, U. (2008) *Hum. Mol. Genet.* **17**, 71-86

86. Tian, G., Zhou, Y., Hajkova, D., Miyagi, M., Dinculescu, A., Hauswirth, W. W., Palczewski, K., Geng, R., Alagramam, K. N., Isosomppi, J., Sankila, E. M., Flannery, J. G., and Imanishi, Y. (2009) *J. Biol. Chem.* **284**, 18980-18993

87. Mustapha, M., Chouery, E., Chardenoux, S., Naboulsi, M., Paronnaud, J., Lemainque, A., Megarbane, A., Loiselet, J., Weil, D., Lathrop, M., and Petit, C. (2002) *Eur. J. Hum. Genet.* **10**, 210-212

88. Ebermann, I., Scholl, H. P., Charbel Issa, P., Becirovic, E., Lamprecht, J., Jurklies, B., Millan, J. M., Aller, E., Mitter, D., and Bolz, H. (2007) *Hum. Genet.* **121**, 203-211

89. Yang, J., Liu, X., Yue, G., Adamian, M., Bulgakov, O., and Li, T. (2002) *J. Cell Biol.* **159**, 431-440

90. Mburu, P., Mustapha, M., Varela, A., Weil, D., El-Amraoui, A., Holme, R. H., Rump, A., Hardisty, R. E., Blanchard, S., Coimbra, R. S., Perfettini, I., Parkinson, N., Mallon, A. M., Glenister, P., Rogers, M. J., Paige, A. J., Moir, L., Clay, J., Rosenthal, A., Liu, X. Z., Blanco, G., Steel, K. P., Petit, C., and Brown, S. D. (2003) *Nat. Genet.* **34**, 421-428

91. Yang, J., Liu, X., Zhao, Y., Adamian, M., Pawlyk, B., Sun, X., McMillan, D. R., Liberman, M. C., and Li, T. (2010) *PLoS Genet.* **6**, e1000955

92. Delprat, B., Michel, V., Goodyear, R., Yamasaki, Y., Michalski, N., El-Amraoui, A., Perfettini, I., Legrain, P., Richardson, G., Hardelin, J. P., and Petit, C. (2005) *Hum. Mol. Genet.* **14**, 401-410

93. van Wijk, E., van der Zwaag, B., Peters, T., Zimmermann, U., Te Brinke, H., Kersten, F. F., Marker, T., Aller, E., Hoefsloot, L. H., Cremers, C. W., Cremers, F. P., Wolfrum, U., Knipper, M., Roepman, R., and Kremer, H. (2006) *Hum. Mol. Genet.* **15**, 751-765

94. Kersten, F. F., van Wijk, E., van Reeuwijk, J., van der Zwaag, B., Marker, T., Peters, T. A., Katsanis, N., Wolfrum, U., Keunen, J. E., Roepman, R., and Kremer, H. (2010) *Invest. Ophthalmol. Vis. Sci.* **51**, 2338-2346

95. Luby-Phelps, K., Fogerty, J., Baker, S. A., Pazour, G. J., and Besharse, J. C. (2008) *Vision Res.* **48**, 413-423

96. Sale, W. S., Besharse, J. C., and Piperno, G. (1988) *Cell Motil. Cytoskeleton* **9**, 243-253

97. Reiners, J., and Wolfrum, U. (2006) *Adv. Exp. Med. Biol.* **572**, 349-353

VITA

Rachel Nicole Wright received her Bachelor of Science degree in genetics from Texas A&M University at College Station in 2006. She entered the graduate genetics program at Texas A&M University in August 2008 and received her Doctorate of Philosophy degree in August 2011. Her research interests are neurobiology and inherited retinal degeneration.

Mrs. Wright may be reached at:

Department of Pathobiology
c/o Dr. Michael Criscitiello
Texas A&M University
College Station, Texas 77843-4467